Department of Precision and Microsystems Engineering

Analysis and design of a large-range bistable linear guide with high support stiffness and low parasitic motion

Tom Huijsmans

Report no	:	2023.101
Coach	:	Dr. ir. G. Radaelli
Professor	:	Prof. dr. ir. J.L. Herder
Specialisation	:	Mechatronic System Design
Type of report	:	Master Thesis
Date	:	December 14, 2023

TU Delft

Analysis and design of a large-range bistable linear guide with high support stiffness and low parasitic motion

by

Tom Huijsmans

to obtain the degree of Master of Science
at the Delft University of Technology,
to be defended publicly on December 14, 2023 at 15:00.

Student number: 4555244

Project duration: September 1, 2022 – December 14, 2023

Thesis committee:

Prof. dr. ir. J.L. Herder,	TU Delft, chair
Dr. ir. G. Radaelli,	TU Delft, daily supervisor
Dr. ir. R. van Ostayen,	TU Delft

An electronic version of this thesis is available at http://repository.tudelft.nl/.

TU Delft

Preface

This thesis project marks the end of my time as a student at the TU Delft. Over six years ago I started with the bachelor Mechanical Enginering in Delft, after which I started the High-Tech Engineering track of the Mechanical Engineering master program, which is concluded with this thesis. I had a great time in Delft, met wonderful people and had amazing experiences. It was an educational journey with many challenges, but to get here I had great support and guidance from many people whom I would like to thank.

I would like to thank Giuseppe for the helpful and necessary discussions during the meetings and his guidance along the way. Also, I would like to thank my colleagues at VDL for their support and guidance during my time there. Furthermore, I would like to thank the students I have met along the way in all those years for the nice lunch breaks, long study sessions and the chill sessions which ended the days on a nice note.

Lastly, I want to thank my family, friends and girlfriend for their support and their help to get my mind of the study. It was nice that I could always count on them to complain about bad days or share eureka moments.

Tom Huijsmans
Delft, December 2023

Contents

1 Introduction

To prevent contamination of production processes or research, cleanrooms are designed. Multiple industries, like electronic part production and biotechnology for example [1], make use of these cleanrooms, where minimization of particle generation is desired. To fulfill this desire while working with large-range linear motion mechanisms, the utilization of compliant mechanisms is looked into.

Linear guides offer linear motion, they come in different shapes and sizes, like roller bearings, ball bearings and friction guides. There also is a category of contactless guides, where wear does not occur, like air bearings, hydrostatic guides and electromagnetic guides [2]. However, these mechanisms are, among other things expensive and not compact [3]. Most mechanisms with large linear displacement provide motion where components slide, scrape or rub against each other, to constrain a mechanism to one degree of freedom [4]. These traditional linear motion mechanisms are compact and establish, compared to their size, quite a long range of motion. But there are challenges with these conventional mechanisms, like the need for lubrication and the resulting friction and wear [5]. The inherent friction and play result in limited precision. This has resulted in engineers looking for replacements for mechanical elements in different applications of linear motion mechanisms [6]. These applications are on both the macro and micro/nanoscale, like in the space or precision industry, integrated in sensors, precision robots or scientific instruments for example [7]. One of the alternatives is compliant mechanism technology.

Compliant mechanisms are looked into more and more over time. Their bodies can be monolithic with slender elements that undergo deflection, also called flexures. They introduce motion through elastic deformation [8]. Compliant mechanisms offer some advantages over rigid mechanisms; they do not suffer from backlash or surface wear, there are fewer components, less weight, no friction between components, less energy loss compared to mechanisms with rigid links and decreased costs [9]. However, compliant mechanism technology has challenges that need more investigation for future development. The largest challenge will probably be the relative difficulty in designing and analyzing compliant mechanisms. The limited motions of these mechanisms and a lack of expertise in compliant design compared to traditional mechanical engineering design are among other things also an issue [10].

There are no large-stroke linear guides that include bistability, offer high support stiffness and have low parasitic motion. The ones that are around offer great bistability but their stroke is very limited [11, 12], their accuracy regarding parasitic motion is of no importance [13], have a large stroke but low support stiffness [14] or offer a large stroke, high support stiffness and minimal parasitic motion, but are not bistable [15].

Here, a new design is presented based on a flexure-based linear guide with torsion reinforcement structures, introduced by Rommers [15] because it meets all requirements except for being bistable. It is expected that this new design allows a linear guide to be bistable while maintaining high support stiffness, low parasitic motion and a large stroke. It could offer a harmonious combination of precision and robustness. It eliminates friction and improves reliability and precision. No power is required for the mechanism to be held in position. Its unique characteristics make it an excellent choice for numerous applications, from precision instrumentation to consumer electronics and advanced robotics. A design will be made as a Finite Element Method (FEM) model, which will be parametrically optimized.

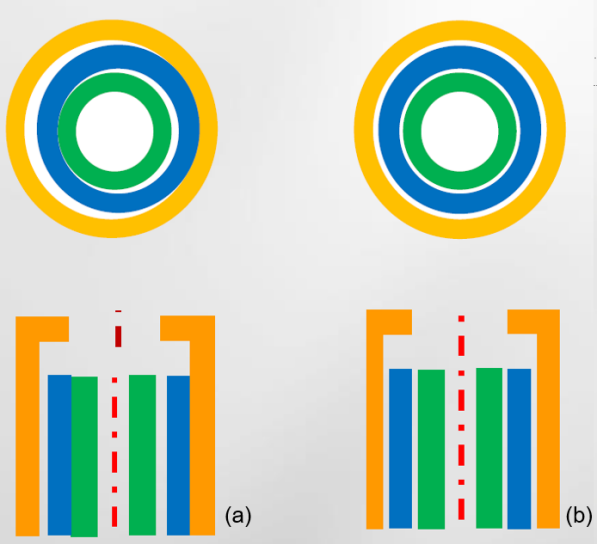

Figure 1.1: Concentric alignment of cylinders with insufficient support stiffness (a) and with proper support stiffness (b).

Experiments will be performed with a prototype to validate the simulation results of the FEA. Finally, a case study will be performed to provide an example for this study.

The case study will be performed for the design of a tool that concentrically aligns two cylinders as can be seen in Figure 1.1. One of the cylinders is a magnet, so magnetic forces must be compensated with support stiffness in the order of magnitude of $10^6 N/m$, and parasitic motion must be no larger than $10\mu m$. A stroke of around $50mm$ is necessary to prepare the shuttle for assembly, the tool must hold the cylinders in place for 72 hours for the glue to dry and the assembly to be finished. To ensure the clamping of the shuttle, bistability is introduced, so it will be forced to the base at a specific position (which holds the other part of the assembly) which makes the assembly possible. The bistable linear guide will not use both stable positions, only the second. To ensure the gluing is possible, the guide will be pressed against the base at its max-force point. This is where the force in the lateral direction will be at its highest to move the guide, so the guide clamping against the base will be best. When its position is altered, the guide will move to its second stable position, where the module can be prepared and the to-be-glued component can be installed. After the preparation of the module, the guide can be positioned back into its max-force point and gluing can retake place. The bistability also makes high repeatability possible, so the tooling will always align the cylinders correctly. It must be possible to place the tooling on a desk and multiple should be able to be stored together so more assemblies can be created, so the smaller the tool the better.

2

Literature review

Literature review on linear motion mechanisms making use of compliant mechanism technology

Tom Huijsmans
Delft University of Technology
Department of Precision Mechanism Design

Abstract— **Compliant linear motion mechanisms are used in a variety of application areas, such as precision stages, biomedical devices, optical precision equipment and aerospace mechanisms. The products range from the macro-scale to micro-electromechanical systems (MEMS). This literature review provides an overview of all current techniques which deliver linear motion while making use of compliant linear motion technology. Research has been done on a variety of mechanisms, but these papers were all very specific and took only some techniques into consideration. There has not been an overview of mechanisms where all different techniques have been taken into account. The classification consists of the methods which deliver this linear displacement, based on plane symmetric, rotational symmetric and asymmetric designs. They all have designs that generate both straight-line and approximate straight-line motion. The mechanisms vary in type of flexures, are based on linkages or make use of bistability. The designs found in articles are discussed and evaluated on their properties, some of which are normalized to make a good comparison. It was found that the best designs have plane or rotational symmetry to deliver straight-line motion. Designs with folded leaf springs look most promising when looking at their displacement per dimensions ratios. For further research rotational symmetric approximate straight-line designs might be interesting to look into, because there are no designs in this category yet.**

I. Introduction

To prevent contamination of production processes or research, cleanrooms are designed. Multiple industries, like electronic part production and biotechnology for example [1], make use of these cleanrooms, where minimization of particle generation is desired. To fulfill this desire with large-range linear motion mechanisms, the utilization of compliant mechanisms is looked into.

Linear guides offer linear motion, they come in all shapes and sizes, like roller bearings, ball bearings and friction guides (see Figure 1). There also is a category of contactless guides, where wear does not occur, like air bearings, hydrostatic guides and electromagnetic guides [2]. However, these mechanisms are, among other things expensive and not compact. Most mechanisms with large linear displacement provide motion where components slide, scrape or rub against each other, in order to constrain a mechanism to one degree of freedom [3].

Fig. 1: A variation of linear motion guides [4].

These traditional linear motion mechanisms are compact and establish, compared to their size, quite a long range of motion. But there are challenges with these conventional mechanisms, like the need for lubrication and the resulting friction and wear [5]. This inherent friction and play result in limited precision. This has resulted in engineers looking for replacements for mechanical elements in different applications of linear motion mechanisms [6]. These applications are on both the macro and micro/nanoscale, like in the space or precision industry, integrated in sensors, precision

robots or scientific instruments for example [7]. One of the alternatives is compliant mechanism technology.

Compliant mechanisms are looked into more and more over time. They mainly have monolithic bodies with slender elements which undergo deflection, also called flexures. They introduce motion through elastic deformation [8]. Compliant mechanisms offer some advantages over rigid mechanisms; the functionality is improved, there are fewer components, less weight, no friction between components, less energy loss as compared with mechanisms with rigid links and decreased costs [9]. However, compliant mechanism technology has its own challenges which need more investigation for future development. The largest challenge will probably be the relative difficulty in designing and analyzing compliant mechanisms. The limited motions of these mechanisms and a lack of expertise in compliant design compared to traditional mechanical engineering design are among other things also an issue [10].

An overview and comparison of current large-range linear motion compliant mechanisms is given by Mackay, [5]. What limits this comparison is that only structures for MEMS are considered, so their comparison is too specific. It does not offer and compare all other alternative techniques which deliver linear motion. Another overview of different compliant mechanisms is given by Huo, [11]. However, this overview compares mechanisms within only one element; different iterations within the same technique. So current research on this subject does not deliver a complete thorough overview of all linear motion techniques which are out there. Researchers have also done some research into compliant rotational joints, [12], [13]. These articles have a similar purpose but a different focus; they look into mechanisms that deliver rotation instead of translation.

The aim of this paper is to display all these different techniques which ensure linear motion with a focus on compliant mechanism technology, to fulfill the desire for minimal particle generation. In addition, the techniques are assessed on their linear displacement compared to their parasitic motion, which requires to be as low as possible.

In Section 2 the obtained literature is described and the search terms that have been used are given, together with the method of how they can be recreated. Also, the classification is explained and the performance criteria are introduced. Section 3 discusses all the found mechanisms and covers the results of the comparison of the different techniques according to the criteria. In Section 4 the discussion of the acquired results is elaborated and in Section 5 the literature review is concluded.

II. Method

A. Literature search

To acquire relevant articles and papers, Google Scholar, ScienceDirect, ResearchGate and Scopus were used. In order to find suitable literature a variety of search terms have been used, these are listed in Table I. These terms are all in line with compliant linear motion mechanisms. To obtain the relevant articles in a systematic way, a search protocol has been used. The terms in the columns can be combined with the terms of other columns to retrieve suitable search terms. The articles that provide a compliant mechanism that produces a straight-line motion have been used for this literature review.

TABLE I: Search terms

	AND			
OR	linear motion	guiding	mechanism	parasitic displacement
	straight-line	large displacement	support stiffness	transverse stiffness
	parallelogram	high precision	PRBM	
	bistable	cylindrical	linkage system	
	axial stiffness	motion range	four-bar mechanism	
	1-DOF	monolithic	structure	
	CFM	stroke		
	flexure			

B. Classification

In engineering, there are a lot of different techniques to acquire linear motion, as stated before. However, for this review, only the mechanisms that supply linear motion, which can be defined as compliant mechanisms are taken into account. In this compliant branch, there is a limited amount of mechanics that ensure linear motion. The categories these different mechanisms can be divided

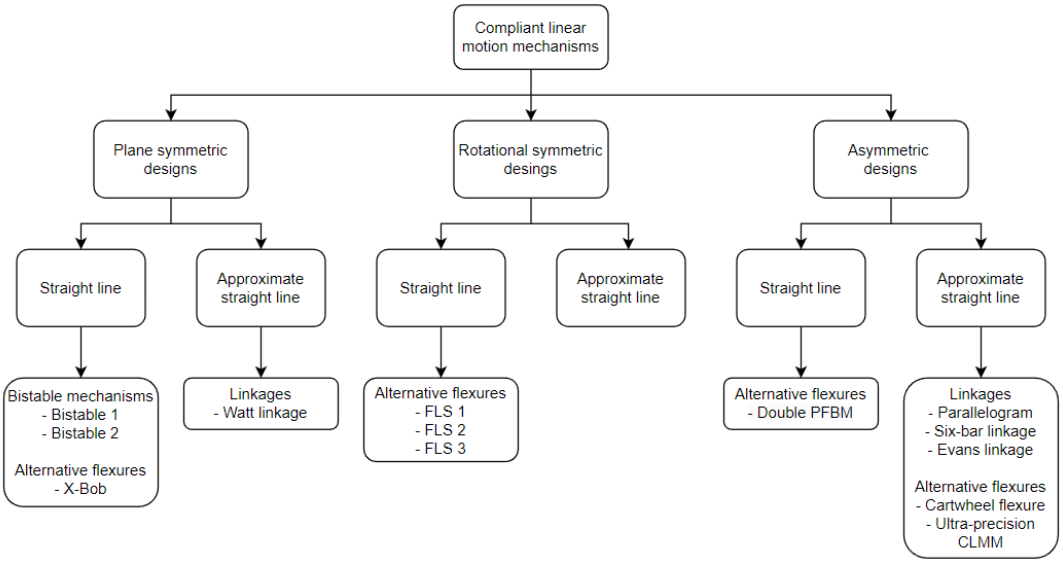

Fig. 2: Categorization literature review.

into are classified by their design. This is regarding the symmetry along the axis of movement of the guiding beam. The classification focuses on 3 types of designs:

1) Plane symmetric designs: A plane of symmetry divides a design into two parts that are mirror images of each other.

2) Rotational symmetric designs: A design is rotational symmetric if it is rotated around a center point (less than a full rotation) and it still appears the same as it did before the rotation.

3) Asymmetric designs: A design that is not symmetric is said to be asymmetric. This means the asymmetric design cannot be divided into identical halves. In addition, because most mechanisms are mostly monolithic and all the elements are connected to each other without conventional joints, there can not be only linear motion. Parasitic motion also comes into play. This is unwanted motion perpendicular to the linear motion which is wanted. This leads to a division of the designs into *straight-line* and *approximate straight-line mechanisms*. This division will categorize all found mechanisms. A schematic overview of this categorization is provided in Fig. 2.

C. Performance criteria

To attain the best-performing technique some performance criteria are determined. The reviewed mechanisms have different application areas. Some techniques are being deployed in MEMS, which means they are in the order of magnitude of micrometers. Other techniques are being used in an order of magnitude of centimeters as in biomechanics. Some values need to be normalized so that the orders of magnitude can be compared. The results of the discussed articles which are of importance for this review will be categorized and presented in a table.

The following criteria are selected:

1) Force: The input force to make the actuation possible.

2) Linear displacement: This criterion is the motion in the wanted direction, the larger the linear displacement, the better the technique.

3) Parasitic motion: This criterion is the motion in the unwanted direction, perpendicular to the direction of movement of the wanted linear displacement. The lower the parasitic motion the better. However, the designs that deliver straight-line motion do not produce parasitic displacement.

4) Transverse stiffness: The transverse stiffness (or support stiffness) is the stiffness in the direction perpendicular to the linear displacement direction. The higher the transverse stiffness the better.

5) Axial stiffness: The axial stiffness is the stiffness in the direction parallel to the linear displacement direction. The lower the axial stiffness the better.

6) Dimensions: The size of the mechanism can be described by the diagonal of the bounding box, of which the lengths are defined by the longest and widest instances.

III. Results

All mechanisms found will be discussed in this section. The designs will be described and evaluated first, whereafter they will be compared to one another with numerical values.

A. Plane symmetric straight-line designs

Bistable mechanisms. Compliant mechanisms can achieve bistability which results in precise state positions. They are flexible devices with two stable equilibrium states within their range of motion [14]. The guiding beam, or shuttle, which is being moved into these positions can be resting in either of two states. The beginning and end positions of the reviewed mechanisms are on-axis aligned. In Fig. 3 a fabricated compliant bistable mechanism is shown. Zirbel evaluates multiple iterations of this design [15]. The iterations vary in the thicknesses of the addition of the thicker middle sections of the flexible (compliant) beams. These sections improve the stability of the mechanism because the flexible beams are being directed toward a better-defined motion. Because the bistable action force is slightly increased by the thicker sections, the mechanism is being helped to hold the second stable position. However, the addition of thicker sections also leads to increased stress in the mechanism. Different thicknesses have been evaluated and an optimum thickness of 30,5 mm was chosen, which had the lowest stress at the most vulnerable position during displacement.

Fig. 3: A bistable mechanism in its fabricated position [15].

The compliant chevron-type mechanism shown in Fig. 4 has besides the normal flexures (curved beams in the figure) also lateral beams. The joint of the lateral beams and the outer curved beam works the same as a flexible hinge and makes it possible for the mechanism to move. To prevent twisting during linear movement of the guiding beam (shuttle mass in the figure), a guide beam (see figure) which is designed to be stiff is introduced. When enough force on the shuttle mass is exerted the lateral and curved beams deflect and then the mechanism snaps into its second stable equilibrium state. The mechanism is designed in a way that the beams have optimal curves in the rest state so that the flexible hinges store a large part of the strain energy. This leads to the mechanism being able to act as a means of protection, in the event of sudden overloading or a mechanical shock for example [15], [16].

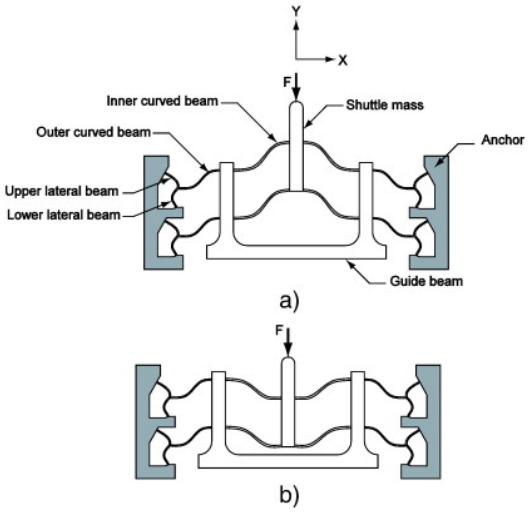

Fig. 4: A bistable mechanism in both equilibrium states [16].

Alternative flexures. The basic compliant parallel four-bar mechanism's flexible beams, as can be seen in Fig. 11, can be swapped with different beams. They are essentially flexural building blocks with different constructions, like a cross-spring pivot for example. Multiple iterations of cross-spring flexures are designed. The center shift of this generalized pivot is utilized, so that inherent parasitic motion can be compensated [17].

MacKay compares multiple mechanisms where the design in Fig. 5 delivers the largest displacement [18]. On top of that, the design has proven to be effective in the area of MEMS. This X-

Bob design is comprised of a center shuttle with a compliant suspension. The X-Bob was designed to allow a unidirectional displacement of the center shuttle.

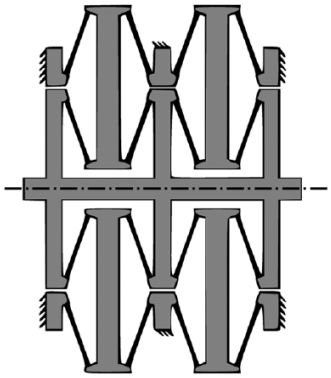

Fig. 5: X-Bob design [18].

B. Plane symmetric approximate straight-line designs

Linkages. Another way to achieve a linear motion is by making use of linkages. A linkage is a rigid-body mechanism consisting of multiple bars which can translate a point or body, which follows a certain path or motion. So the translation of a link or point can be acquired by this technology with well-known rigid-body linkages. For this paper, the compliant counterpart of these linkages will be focused upon [19]. In Fig. 6 the conventional Watt four-bar linkage is shown. The coupler point C in the figure is in the middle of the coupler AB. Point C can be guided on an approximate rectilinear path segment which is presented as the red line in the figure.

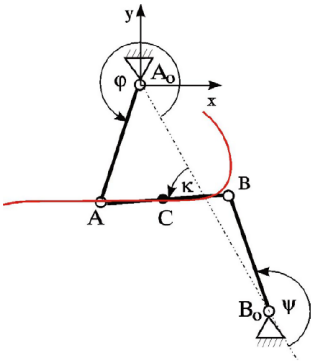

Fig. 6: The Watt four-bar linkage for rectilinear guiding of coupler point C [19].

Fig. 7 shows the compliant counterpart of the Watt mechanism which realizes parallel guiding. Instead of a point like in the original Watt linkage, the entire segment C, the connecting link, in the figure is being guided. This is due to the fact that the compliant compound mechanism is made up of two single compliant Watt mechanisms. This means couplers AB and A'B' are realizing the translation of the planar displacement of connecting link C. This is because the planar displacements of all the points of the connecting link are roughly equal. This realizes parallel-guiding of the link of this compliant Watt mechanism, resulting in a guiding accuracy better than its rigid-body variant.

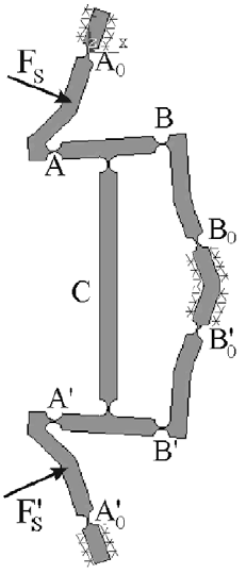

Fig. 7: Compliant counterpart of the Watt four-bar linkage for translation of the connecting link C [19].

C. Rotational symmetric straight-line designs

Alternative flexures. This mechanism again makes use of the basic parallelogram, but they are applied in another way. The flexure elements are now leaf springs and folded, to maintain a high support stiffness in an actuated state. Folded leaf springs can be used in order to obtain stiffness in one direction and have no parasitic displacements [20]. A commonly used compliant linear guide in industry, existing of six folded leaf springs is shown in Fig. 8 [21]–[23]. In the fabricated position of the flexures, which is the initial state

of this design, the support stiffness is high [24]. They allow their motion by bending deformations. The parts at the end of the leaf springs are fixed to the world. This design provides low stiffness along the actuated direction, while a high support stiffness is present in the other five spatial degrees of freedom of the guiding beam.

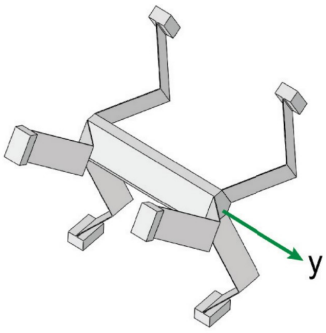

Fig. 8: A compliant linear guide with six folded leaf springs [24].

The design of Rommers, [24], builds on this mechanism of Fig. 8 with a combination element. The proposed design makes use of a combination of a pre-curved folded leaf spring and a straight (regular) folded leaf spring, see Fig. 9. Because of this combination, the support stiffness is high in both the beginning and end positions of the guiding beam. This is due to the fact that in both states there are flexures in their straight orientation. This combination offers the highest support stiffness while ensuring the largest displacement. Only two straight folded leaf springs or only pre-curved folded leaf springs result in either a smaller displacement or offer a lower support stiffness.

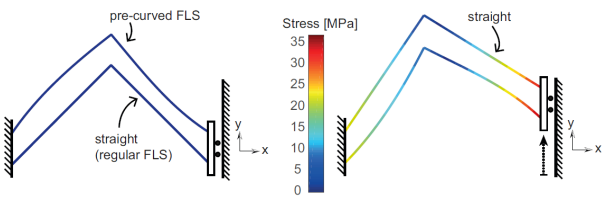

Fig. 9: The combination element with a straight and pre-curved flexure in both beginning and end position [24].

D. Asymmetric straight-line designs

Alternative flexures. This design of Rommers shows a different straight-line motion mechanism, with torsion-reinforced folded leaf springs [25]. The addition of the fins on both folded leaf springs ensures torsion reinforcement, while the combination of the leaf springs in different planes perpendicular to each other ensures the straight-line motion.

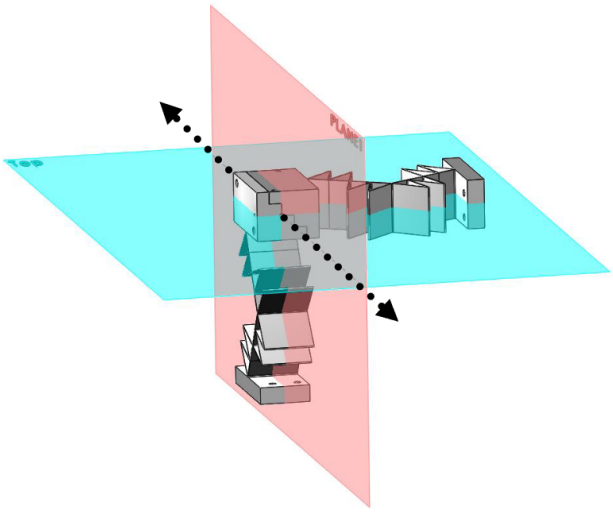

Fig. 10: A large range spatial linear guide with torsion reinforcement structures [25].

E. Asymmetric approximate straight-line designs

Linkages. A parallelogram mechanism is a special form of a four-bar linkage and is one of the most classic forms of parallel guiding mechanisms, namely a parallel four-bar mechanism. It has a simple structure, can easily be manufactured and can be used for both translational and rotational motions. However, in this case, only the translational precision motion will be looked into [26]. The mechanism consists of two flexures that are connected to one guiding beam that will make a small displacement, which results in linear motion. The two supporting arms of the basic parallelogram in Fig. 11, which are connected to the guiding beam, can be altered. The deformation and stiffness of the mechanism can be adjusted by the length ratio of the flexible and rigid sections. The larger the flexible section (compliant beam in the figure) of the supporting arms is, the larger the linear displacement of the guiding beam will be. This also results in a larger parasitic motion.

Opposite, if the rigid section (rigid beam in the figure) of the support arms is larger, the linear displacement will be smaller, as well as the parasitic motion. The rigid beam is enclosed by two compliant beams. For this design an optimum ratio between the lengths of the rigid and compliant beams is chosen, where there is the largest linear displacement with the relatively smallest parasitic motion. The length of the rigid beam is 50 mm and the length of the compliant beams is 10 mm. The rigid beam is 15 times as wide as the compliant beam. Because this design is a basic parallelogram, not much can be adjusted [26].

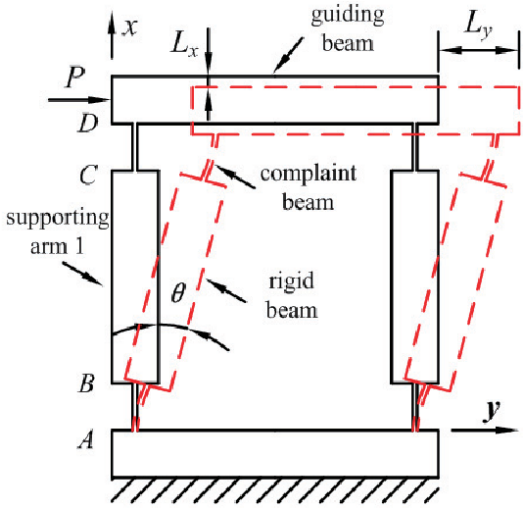

Fig. 11: A compliant parallel four-bar mechanism [26].

Another variant on the basic parallelogram is the double compliant parallel four-bar mechanism as seen in Fig.12. The intermediate stage is added to diminish parasitic displacement. However, this intermediate stage introduces a redundant degree of freedom, which is unconstrained. For dynamic actuation and ambient vibrations this causes issues [27].

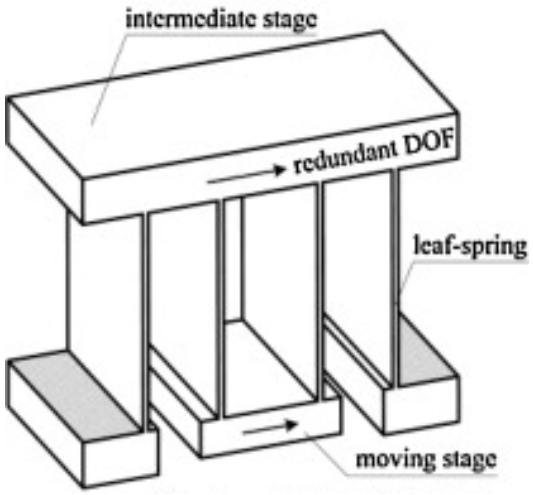

Fig. 12: A double compliant parallel four-bar mechanism [27].

In Fig. 13 the first compliant counterpart of a rigid-body mechanism which is capable of realizing an approximate rectilinear link translation is shown. The dashed lines in the figures represent the links of the rigid-body counterpart. The original six-bar rigid-body linkage realizes a parallel motion of the coupler EK in the figure. This compliant variant also translates the coupler EK. When the mechanism is moving, the coupler is always parallel to its previous position. For the original linkages, an input crank rotation is necessary in order to acquire the correct movement of the linkage. For the scope of this review, these details of this concept are being omitted, and just the values and principles of the parts that ensure linear motion are being looked into. The guiding accuracy of the compliant variant is similar to the rigid-body variant, the decent values of displacement and parasitic motion are the same.

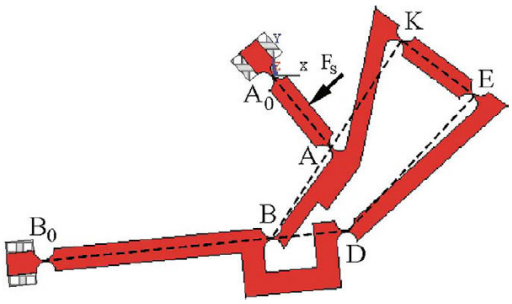

Fig. 13: Compliant counterpart of the six-bar rigid-body mechanism for parallel movement of coupler EK [19].

On the basis of the Evans four-bar linkage shown in Fig. 14 multiple six-bar rigid-body linkages which realize parallel guiding have been developed. In order for the Evans linkage to work, the length ratio of the links is important and is fixed. The coupler point C can be guided along the approximate rectilinear path segment which is presented as the black line in the figure. The length of this path is almost similar to the lengths of links AC and A_0A, so this can be designed in whatever way is wanted.

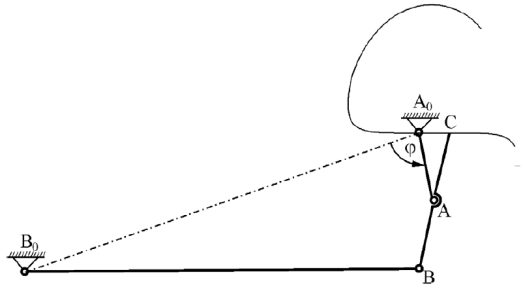

Fig. 14: The Evans four-bar linkage for rectilinear guiding of coupler point C [19].

Of one of the six-bar rigid-body linkages, a compliant variant is designed which is shown in Fig. 15, where the dashed lines again represent the rigid-body variant. The mechanism realizes the link translation of coupler EG. If the input force is located in the middle of coupler BB_0 the best-guiding accuracy can be established. However, for this design, the rigid-body variant has better-guiding accuracy compared to the compliant variant.

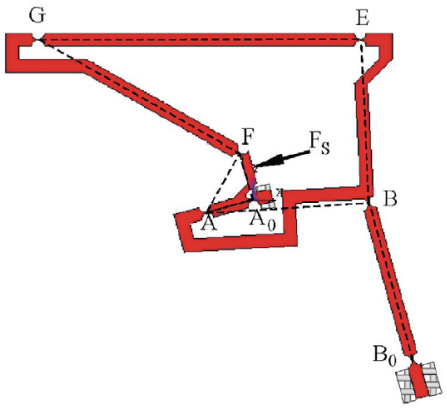

Fig. 15: Compliant counterpart of the Evans four-bar linkage for translation of link EG [19].

Alternative flexures. Fig. 16 shows the design with the cartwheel flexural building blocks. The design combines two triangle flexural pivots in series, which should decrease the parasitic displacement.

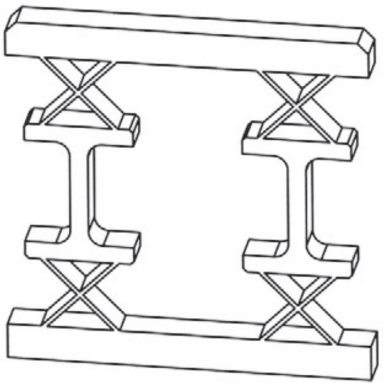

Fig. 16: Design with cartwheel flexural building blocks [17].

Fig. 17 shows the mechanism when it is displaced.

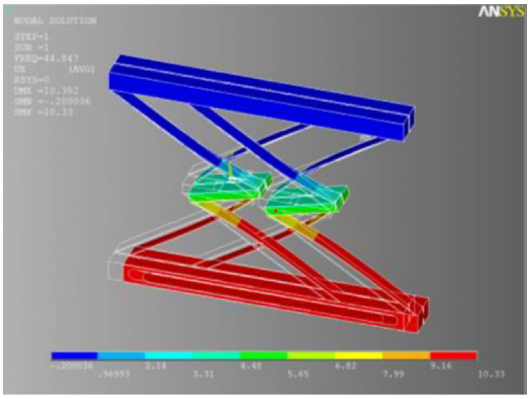

Fig. 17: The cartwheel flexural mechanism in its actuated state [17].

In Fig. 18 an ultra-precision compliant linear motion mechanism with a translational flexural pivot is shown. It makes use of multiple flexures connected by intermediate stages. The introduction of the flexural pivots with their center shift ensures a large linear displacement with a reduced parasitic displacement [27].

TABLE II: Comparison of mechanisms

Article	Type	Force	Displacement	Parasitic motion	Transverse stiffness	Axial stiffness	Dimensions
[16]	Bistable 1	-	5 mm	-	-	-	168.9 mm
[15]	Bistable 2	-	27 mm	-	-	-	207.8 mm
[18]	X-Bob	14 μN	250 μm	-	1.83 $\mu N/\mu m$	0.028 $\mu N/\mu m$	2369 μm
[19]	Watt linkage	-	-	39 nm	-	-	-
[24]	Folded leaf spring 1	-	12 mm	-	4.8 N/mm	-	186.6 mm
[24]	Folded leaf spring 2	-	20 mm	-	4.8 N/mm	-	186.6 mm
[25]	Folded leaf spring 3	-	30 mm	-	20 N/mm	-	182.5 mm
[26]	Basic parallelogram	10N	454 μm	1.75 μm	-	-	99.1 mm
[27]	Double PFBM	-	6 mm	-	4.8 N/mm	-	108.3 mm
[19]	6-bar linkage	-	5 mm	320 μm	-	-	-
[19]	Evans linkage	40N	5 mm	0.1 mm	-	-	353 mm
[17]	Cartwheel	-	0.15 mm	35 μm	-	-	70.7 mm
[27]	Ultra-precision CLMM	-	5 mm	0.24 mm	-	-	114 mm

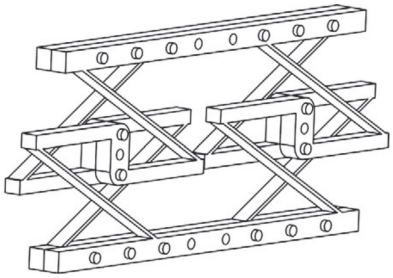

Fig. 18: A ultra-precision compliant linear motion mechanism [27].

Fig. 19 shows the mechanism when it is displaced.

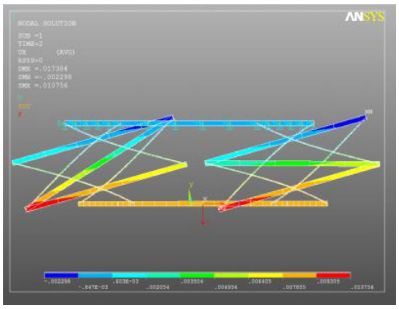

Fig. 19: The ultra-precision compliant linear motion mechanism in its actuated state [27].

F. Comparison of different concepts

An overview of the values of the found mechanisms is presented in Table II. Unfortunately, the values of the stiffnesses were not noted everywhere, but the linear displacement with its parasitic motion and the dimensions for the diagonal of the bounding box were given and these give a good representation. Other values in the table can be normalized by dividing the value with the dimension criteria, to compare the orders of magnitude. Table III shows the relevant normalized values of the displacement and parasitic motion and dimensions ratios. As stated before, all designs that deliver straight-line motion do not have parasitic motion.

TABLE III: Normalized values of displacement and parasitic motion ratio and of displacement and dimensions ratio.

Type	Displacement/ Parasitic motion	Displacement/ Dimensions
Bistable 1	-	0.029
Bistable 2	-	0.13
X-Bob	-	0.11
Watt linkage	-	-
Folded leaf spring 1	-	0.0643
Folded leaf spring 2	-	0.107
Folded leaf spring 3	-	0.164
Basic parallelogram	259.4	4.6e-3
Double PFBM	-	0.055
6-bar linkage	15.6	-
Evans linkage	50	0.014
Cartwheel	4.3	2.1e-3
Ultra-precision CLMM	20.8	0.044

The concepts that are designed to deliver straight-line motion have a good displacement per dimensions ratio compared to the concepts that deliver approximate straight-line motion. The rotational symmetric designs deliver the best displacement per dimensions ratio. The folded leaf spring designs have a displacement per dimensions order of magnitude gap of 10, which is very beneficial. The bistable mechanisms and X-Bob have no valued parasitic motion, so a displacement per parasitic motion ratio can not be given. How-

ever, the values of the stroke with respect to the dimensions are significantly larger, with only an order of magnitude gap of 10-100. The concepts that are designed to deliver approximate straight-line motion face parasitic displacement, where the basic parallelogram shows a good displacement per parasitic motion ratio. However, the dimensions of the mechanism with respect to the values of the stroke, there is an order of magnitude gap of 1000, which is very detrimental. The compliant linkages unfortunately did not offer a lot of dimensions, but their displacement per parasitic motion ratio looks promising. The asymmetric designs that are designed to deliver approximate straight-line motion offer the lowest ratios for both displacement per parasitic motion as per dimensions. Because of the lack of values given for the parameters of the design, a definitive fair conclusion can not be given. In order to do this first the designs should be experimented on. But in terms of the displacement per parasitic motion ratio, the linkages are worth looking into, while for the displacement with respect to the dimensions order of magnitude gap, the folded leaf spring designs look most promising.

IV. Discussion

This review presents linear motion mechanisms making use of compliant mechanism technology. However, a lot of the articles only show concept designs. In just some of these articles, the concept design is calculated with or experimented on, which results in the actual values. These have been discussed.

To achieve the two equilibrium points with a bistable mechanism, it is expected that the movement will be symmetrical. The enclosed guiding beam will move from its beginning to its end position. It follows a linear path with halfway maybe a small kink, but is supposed to end up on the same axis as where it started. For the basic bistable mechanism with 2 flexures on each side, this small kink can occur and is an unwanted movement. To prevent such movement, multiple flexures on each side can be introduced, this way the movement of the flexures will more or less be symmetrical

Folded leaf spring design has the same issue, the movement is linear because of the way the guiding beam is enclosed, so the parasitic motion does not have to be taken into account. This does not necessarily mean that these are then the best options, due to the fact that they each have their own limitations. For the folded leaf spring flexures for example, the support stiffness is the most important value. This is of course in some way related to the parasitic motion, but not measurable in the same way. But because the mechanism is structured the way it is, the support stiffness is the variable to look into for evaluating the mechanism.

The compliant counterparts of rigid-body linkages is an interesting field. They often work with link ratios in order to acquire the correct movement, so these can be chosen with values that are preferred. Only a few linkages were converted into compliant mechanisms, so this maybe is an opening to look into other rigid-body linkages which can become compliant.

The plane and rotational symmetric designs offer the best mechanisms to achieve straight-line motion without parasitic motion. This is because of the way they are designed, they make use of this symmetry for the path of the guiding beam. However, there are no designs for rotational symmetric approximate straight-line designs, so this can still be looked into.

Unfortunately, for some concepts, only some of the variables and parameters were given. Because those articles would only compare certain aspects of the mechanisms, so for instance some dimensions of some concepts are not relevant for the design that will be evaluated later on in the paper.

V. Conclusion

The objective of this review is to provide an overview of all linear motion mechanisms making use of compliant mechanism technology. All mechanisms that deliver this linear motion found in articles and papers are showcased in this review. A classification of the types of mechanisms has been given and the designs are compared with each other by some performance criteria. The classification consists of the techniques used to acquire this linear motion. The mechanisms are divided into the categories plane symmetric designs, rotational symmetric designs and asymmetric designs. Designs of all of these mechanisms have

been discussed. They are compared with different performance criteria, to give an impression of how well they perform as a compliant linear motion mechanism. The asymmetric designs deliver the lowest displacement or highest parasitic motion, so these are the worst option to create a compliant linear motion mechanism. The plane and rotational symmetric designs prove to be the best option for designing compliant linear motion mechanisms.

REFERENCES

[1] SOS Cleanroom. Industries that use cleanrooms, 2019. Available at https://www.soscleanroom.com/blog/industries-that-use-cleanrooms.

[2] Sanidrives. Which linear guide is most suitable for my application?, 2021. Available at https://sinadrives.com/en/which-linear-guide-is-most-suitable-for-my-application.

[3] Compliant Mechanism Research Group Brigham Young University. Compliant mechanisms explained. Available at https://www.compliantmechanisms.byu.edu/about-compliant-mechanisms.

[4] The Mark of Linear Motion. Linear motion guides. Available at https://www.thk.com/?q=us/node/5197.

[5] Allen B Mackay. Large-Displacement Linear-Motion Compliant Mechanisms Large-Displacement Linear-Motion Compliant Mechanisms BYU ScholarsArchive Citation BYU ScholarsArchive Citation. Technical report, 2007.

[6] Shuvam Senapati. Fascinating world of compliant mechanisms, 2017. Available at https://ieee.nitk.ac.in/blog/compliant-mechanisms.

[7] Solehuddin Shuib, M.I.Z. Ridzwan, and A.H. Kadarman. Methodology of Compliant Mechanisms and its Current Developments in Applications: A Review. *Compliant Mechanism Applications*, 2007.

[8] Kee Bong Choi and Doo Hyeong Kim. Monolithic parallel linear compliant mechanism for two axes ultraprecision linear motion. *Review of Scientific Instruments*, 77(6), 2006.

[9] Larry L. Howell. *Compliant Mechanisms*. John Wiley & Sons, 2001.

[10] CMDE Labs. Compliant mechanism: Advantages & challenges, 2021. Available at https://cmdelabs.medium.com/compliant-mechanism-advantages-challenges-27ff4a0e0566.

[11] Tonglong Huo, Jingjun Yu, Hongzhe Zhao, and Xian Wei. A Family of Novel Compliant Linear-Motion Mechanisms Based on Compliant Rolling-Contact Element Pivot. *Journal of Mechanisms and Robotics*, 14(4), 8 2022.

[12] Y.M. Moon, B.P. Trease, and S. Kota. Design of Large-Displacement Compliant Joints. *Compliant Mechanisms*, 2005.

[13] D. Farhadi, N. Tolou, and J.L. Herder. A Review on Compliant Joints and Rigid-Body Constant Velocity Universal Joints Toward the Design of Compliant Homokinetic Couplings. *Compliant Mechanisms*, 2015.

[14] Leo Zimmerman. What is bistability?, 2023. Available at https://www.allthescience.org/what-is-bistability.htm.

[15] Shannon A. Zirbel, Kyler A. Tolman, Brian P. Trease, and Larry L. Howell. Bistable mechanisms for space applications. *PLoS ONE*, 11(12), 12 2016.

[16] Huy-Tuan Pham and Dung-An Wang. A constant-force bistable mechanism for force regulation and overload protection. *Mechanism and Machine Theory*, 46(7):899–909, 7 2011.

[17] Hongzhe Zhao, Shusheng Bi, and Jingjun Yu. A novel compliant linear-motion mechanism based on parasitic motion compensation, 4 2012.

[18] Allen B. MacKay, David G. Smith, Spencer P. Magleby, Brian D. Jensen, and Larry L. Howell. Metrics for evaluation and design of large-displacement linear-motion compliant mechanisms. *Journal of Mechanical Design, Transactions of the ASME*, 134(1), 2012.

[19] Nenad T. Pavlović and Nenad D. Pavlović. Compliant mechanism design for realizing of axial link translation. *Mechanism and Machine Theory*, 44(5):1082–1091, 5 2009.

[20] JPE-innovations. Flexure engineering fundamental: Folded leaf spring. Available at https://www.jpe-innovations.com/precision-point/flexure-engineering-fundamental-folded-leaf-spring.

[21] Arjo Bos. Position actuator for the ELT primary mirror. *PhD thesis*, 2017.

[22] L.A Cacace. An Optical Distance Sensor: Tilt robust[...]. *PhD thesis*, 2009.

[23] Herman Soemers. *Design Principles for precision mechanisms*. University of Twente, 2011.

[24] J. Rommers and J. L. Herder. Design of a Folded Leaf Spring with high support stiffness at large displacements using the Inverse Finite Element Method. In *Mechanisms and Machine Science*, volume 73, pages 2109–2118. Springer Science and Business Media B.V., 2019.

[25] M. Naves J.Rommers, J.L. Herder and D.M. Brouwer. A large range spatial linear guide with torsion reinforcement structures. *Journal of Mechanics and Robotics*, 2021.

[26] Xuefeng Yang, Wei Li, Yuqiao Wang, and Guo Ye. Output displacement analysis for compliant single parallel four-bar mechanism. In *2010 IEEE International Conference on Mechatronics and Automation, ICMA 2010*, pages 1354–1357, 2010.

[27] Zhao Hongzhe, Bi Shusheng, and Pan Bo. Dynamic analysis and experiment of a novel ultra-precision compliant linear-motion mechanism. *Precision Engineering*, 42:352–359, 10 2015.

3

Research paper

Analysis and design of a large-range bistable linear guide with high support stiffness and low parasitic motion

Tom Huijsmans

***Abstract*— The exploration of compliant mechanisms, especially those providing linear motion, has become a central focus in recent engineering research. These mechanisms, characterized by their monolithic bodies and reduced component interactions, present an attractive alternative to traditional rigid mechanisms, having reduced friction, decreased energy losses, and cost efficiencies. Despite these advantages, designing and analyzing compliant mechanisms remain difficult tasks, with particular challenges arising when aiming for large-range linear motion with high support stiffness and minimal parasitic displacement. This study presents a unique design: the combination of a flexure-based linear guide with the features of a bistable compliant switch mechanism. Because a combination of these mechanisms has not been looked into while still offering a long stroke, high support stiffness and minimal parasitic motion. Through Finite Element Analysis (FEA) and subsequent iterations, an optimized model was conceived, prioritizing stiffness and minimizing undesired motions. This optimized design was turned into a 3D printed prototype. The experiments with the prototype confirmed the results of our computational insights, showcasing the parasitic motion of the prototype to be within $1mm$, and its minimum stiffness at least being $10kN/m$ while still having a stroke of $70mm$. A case study has been set up, of which the proof of concept works and is validated.**

I. Introduction

To prevent contamination of production processes or research, cleanrooms are designed. Multiple industries, like electronic part production and biotechnology for example [1], make use of these cleanrooms, where minimization of particle generation is desired. To fulfill this desire while working with large-range linear motion mechanisms, the utilization of compliant mechanisms is looked into.

Linear guides offer linear motion, they come in different shapes and sizes, like roller bearings, ball bearings and friction guides. There also is a category of contactless guides, where wear does not occur, like air bearings, hydrostatic guides and electromagnetic guides [2]. However, these mechanisms are, among other things expensive and not compact [3]. Most mechanisms with large linear displacement provide motion where components slide, scrape or rub against each other, to constrain a mechanism to one degree of freedom [4]. These traditional linear motion mechanisms are compact and establish, compared to their size, quite a long range of motion. But there are challenges with these conventional mechanisms, like the need for lubrication and the resulting friction and wear [5]. The inherent friction and play result in limited precision. This has resulted in engineers looking for replacements for mechanical elements in different applications of linear motion mechanisms [6]. These applications are on both the macro and micro/nanoscale, like in the space or precision industry, integrated in sensors, precision robots or scientific instruments for example [7]. One of the alternatives is compliant mechanism technology.

Compliant mechanisms are looked into more and more over time. Their bodies can be monolithic with slender elements that undergo deflection, also called flexures. They introduce motion through elastic deformation [8]. Compliant mechanisms offer some advantages over rigid mechanisms; they do not suffer from backlash or surface wear, there are fewer components, less weight, no friction between components, less energy loss compared to mechanisms with rigid links and decreased costs [9]. However, compliant mechanism technology has challenges that need more investigation for future development. The largest challenge will probably be the relative difficulty in designing and analyzing compliant mechanisms. The limited motions of these mechanisms and a lack of expertise in compliant design compared to traditional mechanical engineering design are among other things also an issue [10].

There are no large-stroke linear guides that include bistability, offer high support stiffness and have low parasitic motion. The ones that are around offer great bistability but their stroke is very limited [11, 12, 13], their accuracy regarding parasitic motion is of no importance [14], have a large stroke but low support stiffness [15] or offer a large stroke, high support stiffness and minimal parasitic motion, but are not bistable [16].

Here, a new design is presented based on a flexure-based linear guide with torsion reinforcement structures, introduced by Rommers [16] because it meets all requirements except for being bistable. It is expected that this new design allows a linear guide to be bistable while maintaining high support stiffness, low parasitic motion and a large stroke. It could offer a harmonious combination of precision and robustness. It eliminates friction and improves reliability and precision. No power is required for the mechanism to be held in position. Its unique characteristics make it an excellent choice for numerous applications, from precision instrumentation to consumer electronics and advanced robotics. A design will be made as a Finite Element Method (FEM) model, which will be parametrically optimized. Experiments will be performed with a prototype to validate the simulation results of the FEA. Finally, a case study will be performed to provide an example for this study.

The synthesis of this design is as follows. In section 2 the methodology of the concept will be explained, with a description of the model and how the analyses are done. Section 3 shows the results of the simulations and an experimental validation of the FEM models, using the prototype, and compares these. In section 4 these results will be discussed and future research is suggested, followed by section 5 which covers the conclusion of this paper.

II. Method

In this section, the conceptual design will be explained. The prototype for proof of concept will be shown together with the explanation of the real case scenario. After this, the numerical analysis with a FEM model and optimization will be explained. Subsequently, the experimental setup will be presented

A. Design

The design of Rommers, [16], is used as it is a flexure-based linear guide, see Fig. 1. It has

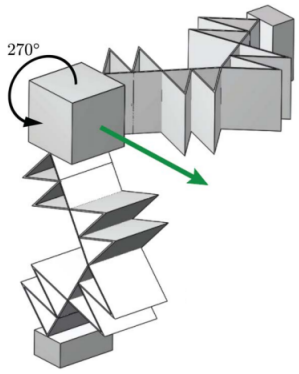

Fig. 1: The linear guide design of Rommers, similar to the well-known rigid link Sarrus mechanism. [16]

torsion reinforcement structures, which ensures the support stiffness is very high compared to how small the flexures are. Moreover, the linear guide moves the shuttle with a large stroke while having this high support stiffness. This means the order of magnitude of the mechanism's size is ideal for the goal of this design. High support stiffness, large stroke and low parasitic motion have been acquired with this mechanism. To obtain bistability a variation on the commonly used compliant mechanism is used, the principle given by Zhao, [13], see Fig. 2.

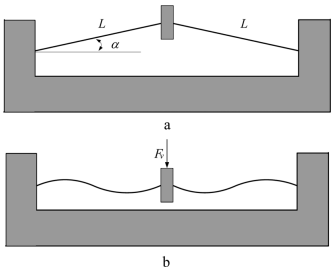

Fig. 2: A clamped-clamped bistable compliant mechanism with both ends clamped. [13]

The mechanism is designed to provide precise state positions. The flexible mechanism has two stable equilibrium positions, while the shuttle in the middle is being guided along the axis of movement in the middle. The parasitic motion is of no concern for the application. The combination

of these principles is the basis of the design for this paper, to check whether the introduction of bistability will reduce support stiffness and increase parasitic motion, while still being able to make a large stroke. Because the shuttle will follow a linear path because of the torsion reinforced linear guide, only one bistable element will be used, as can be seen in Fig. 3.

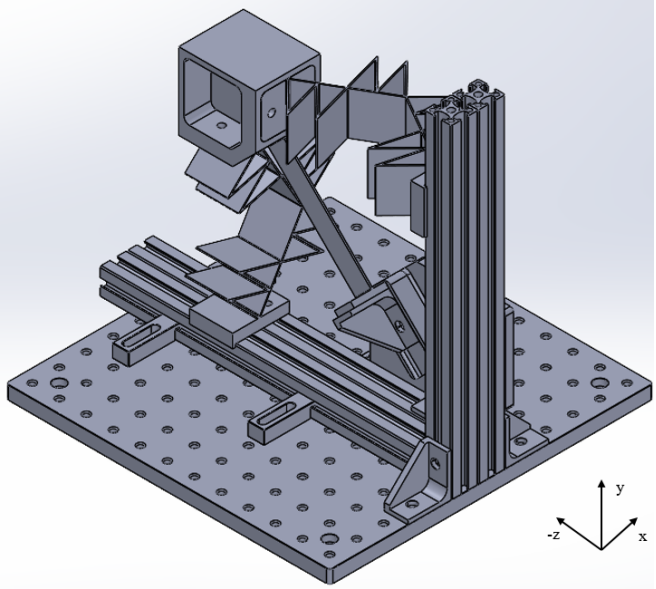

Fig. 3: Solidworks model

The frame around the design would be the base, which must be as stiff as possible. The bistable element can adjusted up and down in the yz-plane, over the axis in the direction of the bistable element. This ensures the bistable element is always secured correctly with respect to the shuttle. Constrained directions are movement in the yz-plane, and rotations around the directions of the x, y and z-axis from the middle of the shuttle. So, this design only allows for movement along the direction of the x-axis from the middle of the shuttle. The bistable element needs to have a preload displacement d for the mechanism to be bistable so that the mechanism will switch to one of its two stable positions. When displacing the shuttle in the correct direction, it will snap to its other stable position.

B. Numerical analysis

In this section, the concept design will be evaluated with a FEM model created in MATLAB. For the FEA, an Euler-Bernoulli beam formulation is used based on the work of Battini [17]. The formulation for linear elastic material uses geometrically non-linear co-rotational beam elements. In the FEM model, the initial geometry is modeled by specifying the coordinates of the nodes of the beam elements. All the leaf flexures have been modeled, including the bistable element and the shuttle. The proposed design has the parameters given as variables, as shown in Fig. 4. To construct the FEM model, the initial dimensions of Rommers' design have been used. For the d and dimensions of the bistable element, an iterative process was employed to fine-tune the values to achieve two stable positions and a max- and min-force point in the force-displacement graph, confirming the mechanism is bistable in the FEM model. The specific values will be assigned in the next subsection.

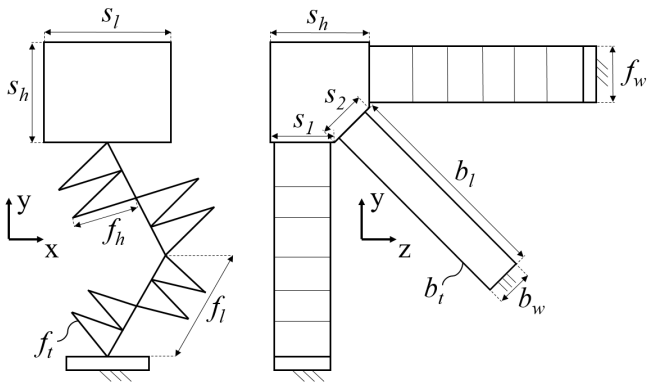

Fig. 4: Parametric design with f_t and b_t being the thickness of the flexures and bistable element respectively.

In the FEA the different components consist of different beam elements. After specifying the node coordinates, the connections between the nodes are assigned. The more beam elements in the components in the design, the more precise simulation can be made, however, this will also result in longer simulation times. So, the critical components of the design where a lot of deformation takes place will be given more beam elements than the components that do not have much influence on the simulation. All the beam elements have a cross-section, which can be defined per element. With this, the concept design is created. Since the design is mainly built of off flexures, the cross-section of these elements can be modeled like rectangles

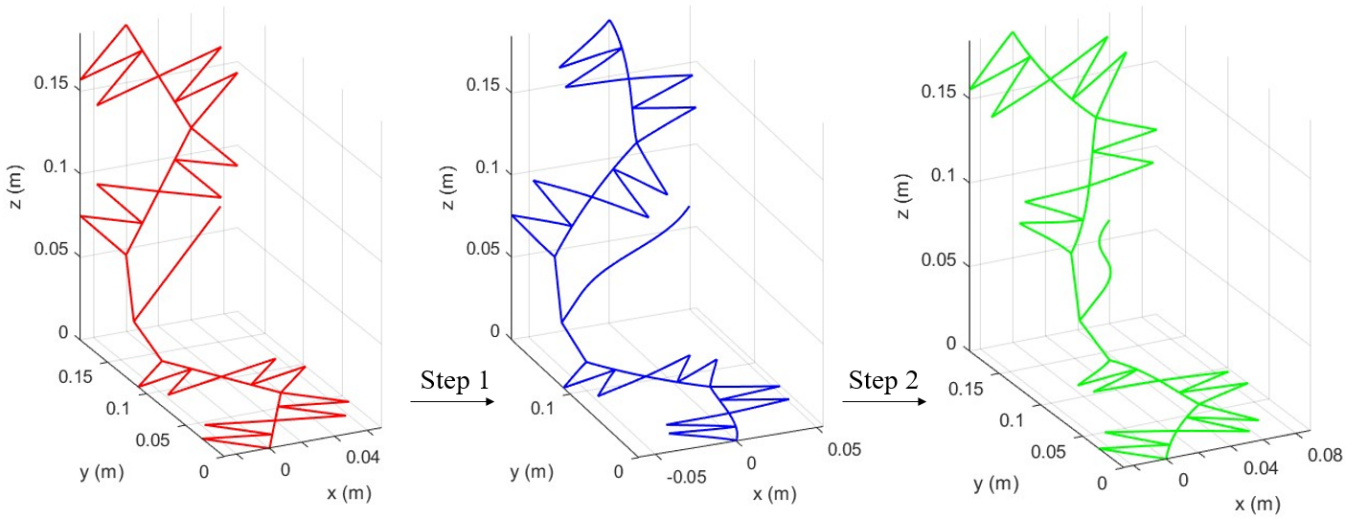

Fig. 5: Stills from the FEA to show the steps of displacement of the mechanism.

or leaf springs. The cross-section of the shuttle is modeled 40 times thicker than the normal flexure because this part will be rigid and must not be able to flex.

Also, material properties are required, so the Young's modulus E and Shear modulus G need to be determined. The values are taken from MakeIt-From [18], a source that gains its information from a survey of technical literature, including both academic books and supplier documentation. They are $E = 3.5GPa$ and $G = 2.4GPa$. However, because the found data is generated of a wide range of values, it might lead to differences in the results from the simulations and experiments. To acquire more accurate values for the material properties, multiple three-point bending tests will be performed on the flexures used in the experiment. The results of these material experiments will be used later in the paper.

After defining the material properties, the boundary conditions will be set. Because it is a 3D model, all nodes have six DoFs (three translational and three rotational). The attachment of the model to the base frame will be modeled as being fully constrained. This happens at the end of the two torsion reinforced leaf flexures. The d of the bistable element enables the linear guide to be bistable, and d determines how big the stroke of the shuttle will be. After this, d is fully constrained as well and the node in the middle of the shuttle will be displaced along the x-axis. One stroke without and one with a pre-force, performed in 100 steps, while for every step the reaction forces and displacements are known. With the known applied pre-force and the resulting positions along the stroke, the support stiffness can be calculated. The parasitic motion along the x-axis can also be calculated per time step. The influence of gravity was neglected in the analysis. Representation of the steps is visible in Fig. 5 for clarification.

The red model is the mechanism before the bistable element is displaced. The blue model is the mechanism when d is added, this is the starting position of the stroke. The green model is the mechanism in its final position after it has completed the stroke.

C. Parametric optimization

In this section, it will be explained how the optimized values for the variables have been found. The following variables, whose values can be found in TABLE I, have been chosen as design parameters: f_t, f_h, b_l, b_h, b_t and d. This means the overall shape of the torsion reinforced flexures will mostly stay unchanged, only the thickness and width will be subject to the optimization. The dimensions of the bistable element and its d are also being optimized. The results from the analysis of the previous subsection are used to generate a force-displacement plot along the x-axis.

The parametric optimization will be done in MATLAB with fmincon, using the sequential

quadratic programming algorithm. The results that need to be optimized are the maximum support stiffness and minimum parasitic motion, while still being bistable.

First was looked at what the boundaries of the variables would be to ensure the mechanism's bistability, which means two stable points and max- and min-force points in the force-displacement graph. The parameters that ensure the bistability are b_l, b_t and d. This entailed using the force-displacement graph and checking the value of the force along the displacement of the x-axis, see Fig. 6.

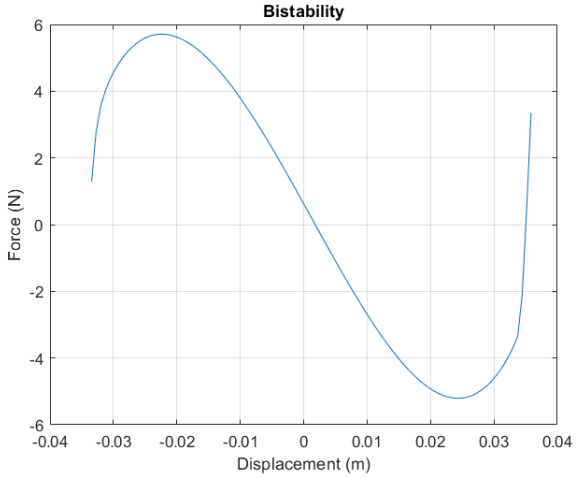

Fig. 6: Plot of wanted behavior for bistability of the mechanism.

For the requirements, a stroke of around 50mm was required. The initial position of the shuttle is the clamping point at the max-force point, so the stroke will start from there. For the design, the distance between the max- and min-force points is set as the required stroke. The value of the peaks was arbitrarily chosen to set a benchmark in order to ensure clamping. It doesn't necessarily have to meet this peak value, as long as the force is high enough for bistability to occur. The dimensional boundaries of the design variables were wide, for the best possible optimization. The initial guess for the values of the design variables was the dimensions based on the values of the design of Rommers.

An objective function, which can be found in Appendix D.1., has been made in order to ensure bistability while looking for the maximum support stiffness in the directions perpendicular to the stroke. The objection function is a combination of three objective components. The first component searches for the maximum stiffness, the second component makes sure the highest value in the graph is the desired force for clamping and the third component makes sure the desired mean of the graph is around zero. The last two components are penalized with weights, to make sure the combination of the components deliver the required optimization. The last two components also ensured boundaries for the bistability, so no unwanted behavior will occur like in Fig. 7. This would lead to an unwanted stroke division, and a gap of around $50mm$ between the force peaks is desired.

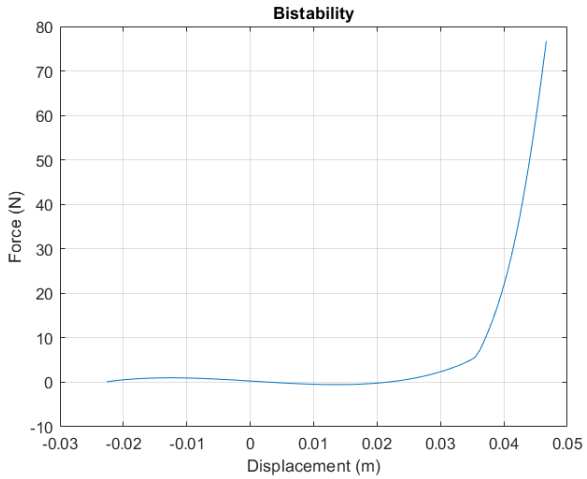

Fig. 7: Plot of unwanted behavior for bistability of the mechanism.

Different weight factors for the penalization have been used in order to acquire a fair optimization, they were iterated so it was made sure every component in the objective function would get a weight accordingly.

To make sure not only one local minimum will be found with a single optimization, the Multistart object is used. This uses multiple initial guesses inside the dimension boundaries in order to find the best value for the objective function. At the end of this process, there is an optimal d, together with optimal values for the other design variables of the model. The optimized dimensions with which the prototype will be manufactured can be found in TABLE I.

Part	Parameter	FEM Dimension (mm)	Measured Dimension (mm)
fin height	f_h	40.00	40.11
flexure length	f_l	80.00	80
flexure thickness	f_t	1.28	1.54
flexure width	f_w	39.97	40
bistable length	b_l	114.98	114.77
bistable width	b_w	20.00	19.85
bistable thickness	b_t	1.60	1.69
pre-displacement	d	9.06	9.07
shuttle to flexure	s_f	50.00	50.00
shuttle to bistable	s_b	30.00	30.00
shuttle height/width	s_w	71.00	71.00
shuttle length	s_l	60.00	60.00

TABLE I: Values of parameters, from FEM and measured.

As stated before with the material properties, the corrected dimensions of the prototype may differ from the optimized values due to manufacturing inaccuracies and tolerances. So the corrected dimensions of the prototype have been measured with a caliper and are listed TABLE I as well.

D. Prototype

A prototype of the design with optimized dimensions will be manufactured for a proof of concept, so the results of the numerical analysis can be validated. The torsion reinforced flexures and bistable element will be 3D printed on the Prusa i3 MK3S+ out of Polylactic Acid (PLA). The part that ensures displacement of the bistable element in the correct direction is also 3D printed. The shuttle is milled from an aluminum block. For the base, Thorlabs rails have been used. The parts are connected to each other with M6 bolts, see a Solidworks model of the prototype in Fig. 3. With a long M6 bolt and a nut, the bistable element can be secured to the 3D printed slide frame. This is in turn also connected to the base. The slide frame through which the long bolt needs to go has a slot for the component that ensures d is correct. It has been designed in a way that different size components can fill the slot, so the desired d can be achieved.

E. Case study

A case study will be performed for the design of a tool that concentrically aligns two cylinders. One of the cylinders is a magnet, so magnetic forces must be compensated with support stiffness in the order of magnitude of $10^6 N/m$, and parasitic motion must be no larger than $10\mu m$. A stroke of around $50mm$ is necessary to prepare the shuttle for assembly, the tool must hold the cylinders in place for 72 hours for the glue to dry and the assembly to be finished. Because of the bistability of the mechanism the shuttle can be clamped to the base frame at a specific position (which holds the other part of the assembly) which makes the assembly possible. For the clamping of the shuttle to the base, the max-force point in the force-displacement graph is used to keep it in place. This is where the force in the lateral direction will be at its highest to move the guide, so the guide clamping against the base will be best. This only holds for the first max-force point, because when the shuttle is snapped to its other stable position, it can be prepared so the assembly can take place. So in practice, the shuttle moves from the max-force point point to the second stable position. See Fig. 8 for clarification.

Because of the form of the torsion reinforced flexures, the mechanism will always move into the same initial stable position, which is in the direction opposite of where the torsion reinforced flexures are pointing (negative x-direction). When its position is altered, the shuttle will move to its second stable position, where the module can be prepared and the to-be-glued component can be installed. After the preparation of the module, the guide can be positioned back into its max-force point and gluing can retake place. The bistability also makes high repeatability possible, so the tooling will always align the cylinders correctly. It must be possible to place the tooling on a desk and multiple should be able to be stored together so more assemblies can be created, so the smaller

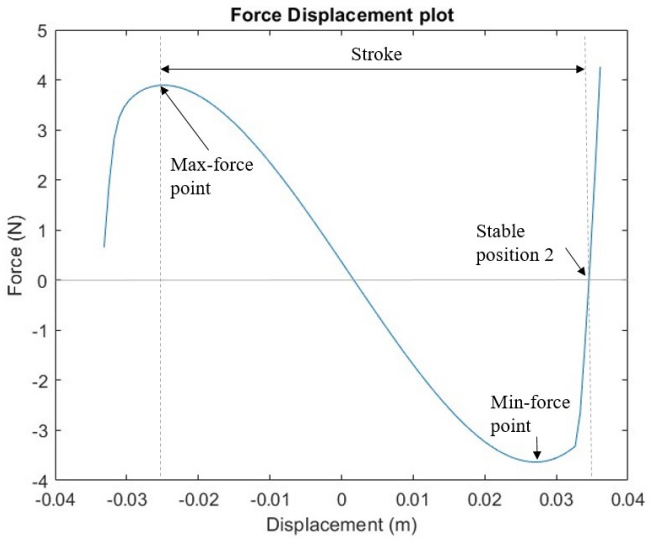

Fig. 8: Force-displacement plot with max- and min-force points and stable position.

the tool the better.

The required stiffnesses and parasitic motions are not achievable with 3D printed parts. The final mechanism would be made entirely out of titanium, so much higher values can be achieved in the required order of magnitude. During this paper, plots with realistic data will be shown, in order to review the case study. For this, commercially pure-grade titanium will be used, with an E-modulus of $120GPa$ and a shear modulus of $45GPa$.

F. Experimental setup

To validate the prototype, an experimental setup is made. The prototype was mounted on Thorlabs breadboard. The displacement along the x-axis will be applied by a translational PI stage, the PI M-505.4DG, which has a range of $100mm$. The resulting reaction forces will be measured by a force sensor, the Futek FSH03875, with a force limit of $45N$. This force sensor is attached to a xy-stage of Thorlabs, so it can be positioned as desired. To connect the shuttle to the force sensor, a fishing line of $0.5mm$ diameter is used. It is light and stiff compared to the measured stiffness in the experiments. Given that the parasitic motion occurs in the yz-plane, perpendicular to the shuttle's direction of travel, this line is chosen so the prototype will not be influenced by undesired forces that could influence the experimental data. On the other side of the shuttle, a mass of $1kg$ is connected via the same type of fishing line and is guided via a pulley. This is done to apply a constant pulling force on the sensor, and the mechanism can be displaced step by step, without moving to either stable position. After installing the bistable element, the lines are so prepared that they are perfectly horizontal and just move the shuttle horizontally. In Fig. 9 an overview of the setup is shown. In text is indicated what the relevant parts are. This

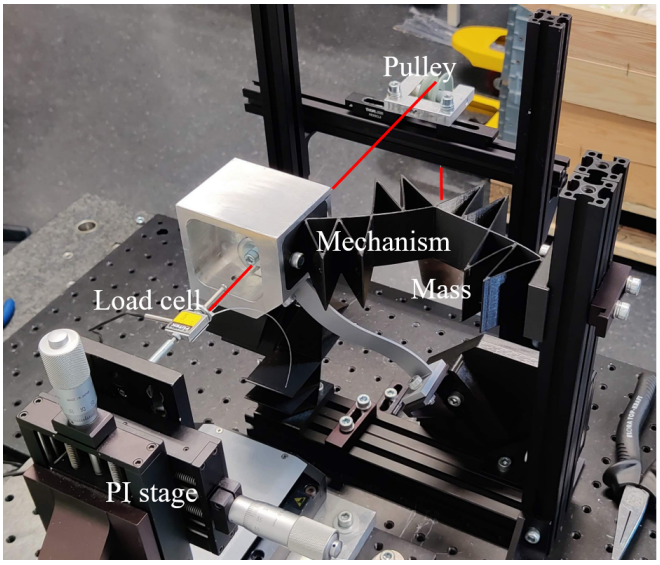

Fig. 9: Experimental setup for bistability

way the forces for bistability can be calculated. A second experiment is performed this way, but now with lasers instead of the force sensor. The micro epsilon lasers optoNCDT 1402 and 1420 have been used to measure the parasitic motion during a stroke. A 3D printed plate was designed to mount the lasers onto the frame of Thorlabs rails. This 3D printed part made sure the middle of the measuring ranges of the lasers would be at the same distance. See Fig. 10 for this setup. 2 lasers have been placed next to each other, so they can measure their relative difference. This way along the entire stroke, the position of the middle of the shuttle can be calculated with trigonometry and inter- and extrapolation, which results in the parasitic motion. Additionally, a weight of $400g$ is placed on top of the shuttle and the parasitic motion was measured again with this pre-force, to recreate the simulation in the numerical analysis where the stiffness could be calculated.

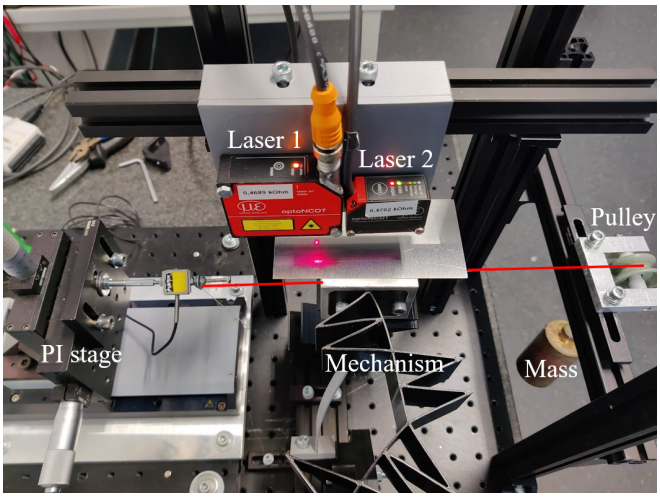

Fig. 10: Experimental setup with the lasers for parasitic motion and stiffness

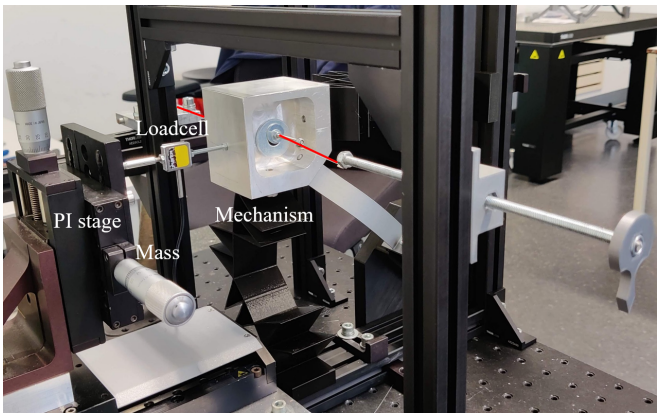

Fig. 11: Experimental setup with loadcell for stiffness

For the last experiment, the mechanism needed to be rotated 90 degrees, so the axis of movement of the shuttle is orthogonal to the direction the PI stage is moving in. See Fig. 11 for the setup. This way, the shuttle could be pressed in by the force sensor, while being displaced step by step along the stroke direction. Now, the shuttle was still attached to a weight on one end, but the other end was attached to a threaded end of size M6 with fishing line. This gave per full rotation of the rod (around its own axis in the lenght) a displacement of 1 mm. So the shuttle could again be guided along the stroke, so measurements could be taken with the force sensor. The force sensor was moving also along the x-axis in the same steps, so the middle of the shuttle will always be pressed. This is possible because the force sensor is attached to a xy-stage. However, the stroke of the xy-stage is only $25mm$, so the PI stage needed to be moved along the x-axis as well, so the setup could be reconstructed again, but now $25mm$ further down the line, so the center of the shuttle can be recalibrated again while the xy-stage was moved in the opposite direction. The point of the force sensor would be placed right in front of the center of the MM. With the PI stage, the tip of the sensor could creep towards the MM per tenth of a millimeter. So the start of the test would be when the tip just touched the surface and then moved one increment back. This way the displacement imposed by the PI stage, which was set op 3mm, would always start in the same condition. This results in a force-displacement graph with which the stiffness can be calculated. The experiments for stiffness and parasitic motion have been conducted with and without the bistable element, for a good comparison between the 2 methods. All experiments have been carried out three times for validity and to reduce uncertainties.

III. Results

In this section, the results will be discussed. All experiments have been performed three times, and an average of these results will be shown in the graphs. There are three types of results; the FEM simulations with optimized dimensions, the experimental results and the FEM simulations with the corrected dimensions. The results are shown both with and without the bistable element. They will be colored blue, orange and yellow respectively in the graphs. They will all be discussed per type of result;

1) FEM simulations with optimized dimensions (green): These results follow from the design with the optimized dimensions, so here the most desired values are achieved. They have no noise and the simulation is always under perfect conditions. This means no external forces, no wrong alignments and no possibility for human errors.

2) Experimental results (blue): To validate the results of the simulations, the prototype is subjected to experimental testing. The prototype has been manufactured as accurately as possible to recreate the exact circumstances.

3) FEM simulations with corrected dimensions (red): Here are the results of the FEM model with corrected values of the prototype displayed. This way the difference between these results and the experimental results can be made quantitative. It is expected that this would lead to results closer to the experimental data.

Extra experiments have been performed to check why there are deviations in the results, for friction in the pulley and stiffness of the base frame. A three-point bending test is performed to find the correct material properties, which are found at $E = 2.418GPa$ for the black and $E = 2.592GPa$ for the grey 3D printed parts. Lastly, the results of the case study are presented as well.

A. Parasitic motion

Here, the parasitic motion of the shuttle's center along the stroke is displayed in Fig. 12b along the x-axis. For all data, the starting position is used as a reference. So of all the positions of the center of the module, the starting position is subtracted. This means all lines in the plot will start at zero on the parasitic motion axis. In grey the upper and lower boundaries of the experimental data are shown. Positive values along the parasitic motion axis mean displacement away from the flexure (positive y-direction), and negative values mean displacement towards the flexure (negative y-direction). The negative displacement starts when the shuttle is halfway through its stroke in all results, before this they are all positive. The parasitic motion in the experiment is within $1mm$ along the entire stroke. The overall shape of the lines is pretty much the same, only the experimental results have a larger deviation in the last $25mm$ of the stroke. However, the results are in the same order of magnitude.

B. Stiffness

For the stiffness, two types of experiments have been performed. One with lasers and one with a loadcell. In Fig. 12d along the x-axis the dark blue line represents the results of the loadcell data and the cyan line the results of the laser data. Now the red line displays the results of the FEM model simulation with corrected dimensions. The data of the laser experiments have more noise, while the force sensor is more steady. The results of the simulations with the corrected data are almost 5 times larger than the results of the experiments. The overall shape of the graphs is quite similar, except for some data of the laser results, where the final part of the stroke has a sudden deviation with a peak in the stiffness. All results are in the same order of magnitude.

C. Bistability

The force of the shuttle is displayed along the stroke it makes, see Fig. 12e. The line of the optimized dimensions is almost point-symmetric around the graph's origin. During the experiment, the shuttle was displaced forward and backward, to check for hysteresis. This is clearly visible in Fig. 12e, there is a force difference between the two strokes. Initially, the force is zero, but when the shuttle is displaced and back at its starting position there is a force difference of $1.50N$. This is roughly the same as most of the force difference of the hysteresis. The values of the peaks of the corrected dimensions are quite close, only the position alongside the stroke is a bit shifted. This only holds for the first stroke of the shuttle, because of the hysteresis. The overall shape of the lines is pretty much the same, while the results of the simulations with corrected dimensions follow the experimental results closely, and all the results are in the same order of magnitude.

D. Simulations and experiments without the bistable element

For the purpose of this paper, the results of simulations and experiments on the design without the bistable element will be checked as well. This will highlight the difference in properties between the original linear guide and the new proposed design. In Fig. 12a it is visible that the beginning and end positions of the shuttle are almost the same. This shows that the bistable element influences the displacement of the shuttle, so it moves in a different path. Also for these results, the relative difference of the initial position to the path of the shuttle has been displayed. In the simulations for the stiffness are peaks present which do not occur during the experiment.

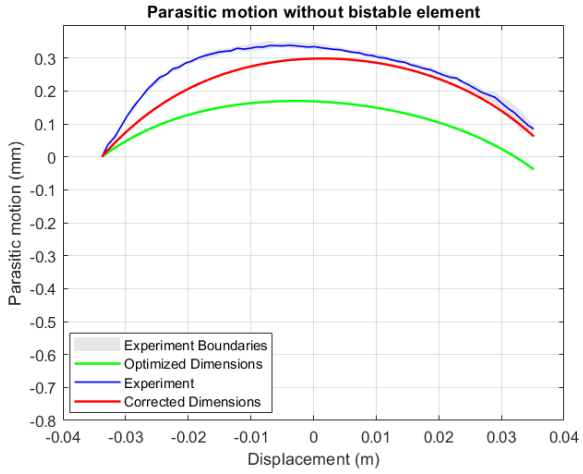

(a) Parasitic motion without bistable element

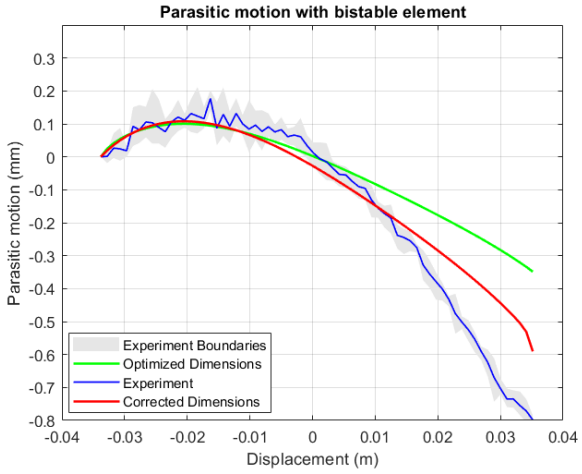

(b) Parasitic motion with bistable element

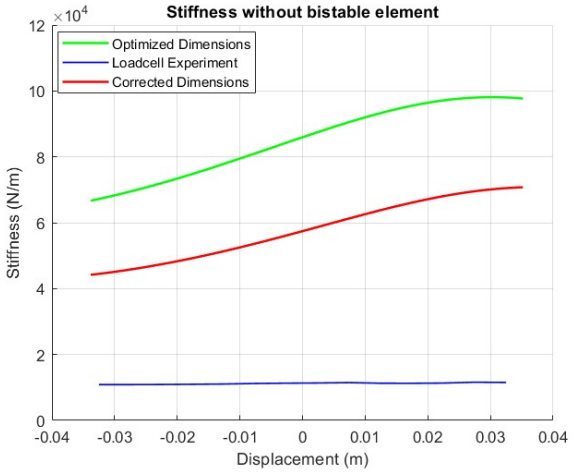

(c) Stiffness without bistable element

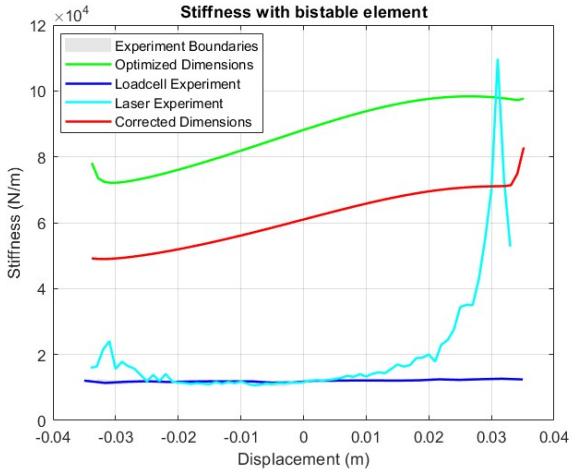

(d) Stiffness with bistable element

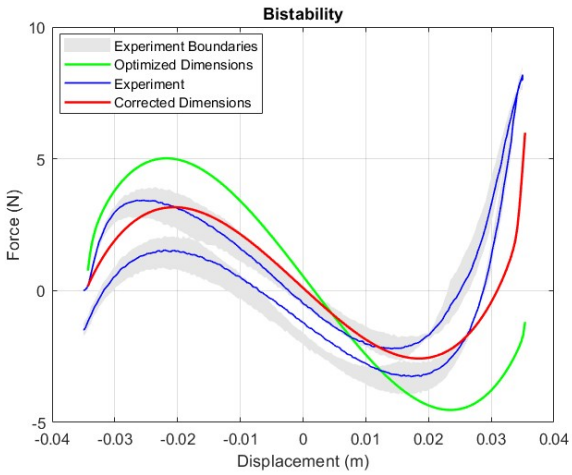

(e) Force displacement graph which shows the bistability of the mechanism

Fig. 12: Plots of the results of FEA and the experiments, with the x-displacement along the y-axis. In a and b the parasitic motion is shown, with and without the bistable element in place. In c and d the stiffness of the mechanism is shown, with and without the bistable element in place. Finally, in e the force-displacement graph is shown which displays the bistability.

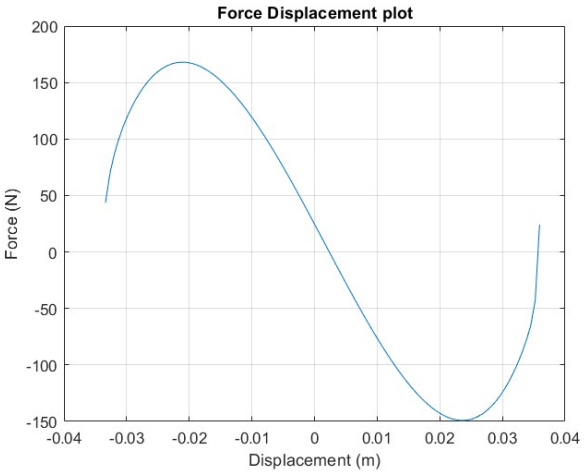

(a) Bistability when the mechanism is made out of titanium.

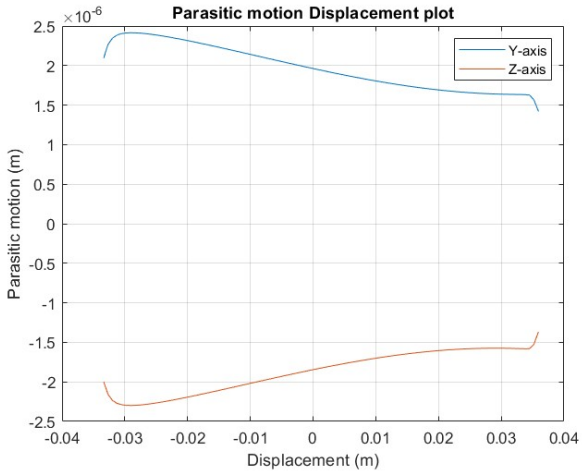

(b) Parasitic motion when the mechanism is made out of titanium.

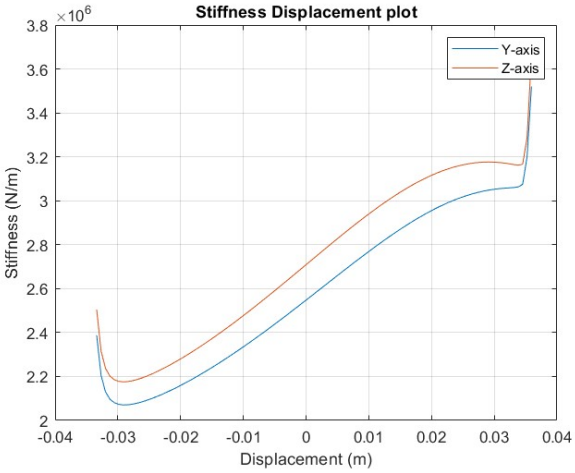

(c) Stiffness when the mechanism is made out of titanium.

Fig. 13: Plots of the results of FEA when the mechanism is made out of titanium..

E. Case study

To fulfill the requirements for the case study parasitic motion and support stiffness of a different order of magnitude are necessary. Making the prototype entirely out of titanium will result in a Young's modulus that is roughly 35 times higher than that of the average found value of PLA, so the requirements of the support stiffness and parasitic motion should be met, see Fig. 13 for results. The parasitic motion is in micrometers (μm) and the support stiffness in meganewton per meter (MN/m). The optimized dimensions of the model have been used.

IV. Discussion

In this section, the results will be discussed, regarding the model itself, the optimization, the experiments and the case study. Finally, some recommendations for future work are given.

A. Design

The introduction of the bistable element expands the function of the original linear guide, and the expected behavior of the mechanism was found in the simulated and experimental results. The mechanism can be bistable while maintaining a high support stiffness and long stroke. The shuttle was manufactured out of aluminum, so it would be possible to have a smooth surface for the lasers and

be very rigid. It was a bit heavier because the part was not 3D printed, while it was already hollowed out. However, due to gravity a little bit of sag of the shuttle occurred, which did not influence the results. The bistable element of the prototype is 3D printed. During these experiments they were under a lot of pressure, so creep occurred, together with plastic deformation after 2 or 3 tests, so multiple bistable elements have been used. It was visible after a few tests that the bistable element was not straight anymore when put beside a square.

B. Optimization

For the optimization, 6 design variables have been addressed, but more variables influence the support stiffness. These are the length and position of the flexures and fins of the torsion reinforcement flexures. Different orientations of the fins can result in other values for the stiffness for example. The reason these were not considered for optimization is that knowledge on this particular design of Rommers is wanted, and optimization on the shape of the flexures would be difficult. The optimized values for the width of the torsion reinforced flexures and the bistable element were both the upper boundaries. The reason this boundary was set is that the shuttle's dimensions were set, in order to hold the components for assembly for the case study. So wider than the upper boundaries was not an option.

C. Experiments

Because two lasers were set up, it was hard to configure the center position of the shuttle. In some way, you are measuring a linear guide with a linear guide. When positioning the rail where the lasers are mounted on, a level was used to make sure the lasers would be level. The slightest angle of this rail can give a deviation in the results. However, if this were the case, the noise would have a relative difference across the entire stroke. The mount that made sure the middle of the measuring ranges of the lasers would be at the same distance was 3D printed, so print inaccuracies of this mount could also cause a small deviation in the distance of the lasers. From the test data, it seemed that there was a slight height difference between the middle of both measuring ranges. In order to account for this, the relative distance of these middles has been calculated and made sure all the data was relative to each other so it was useful for the results. The differences in results might also occur because of the slightly wrong alignment of components during the experiments. Because all parts are manually mounted, human error can cause these differences in the setup, while the simulations are all perfect. The same holds for the stiffness of the setup. Everything is tried to be structured as stiff as possible, but there will always be a margin of error somewhere, so the perfect stiffness as in the simulations can not be recreated. Also, the PI stage can be a reason differences in stiffness are measured, when higher forces are measured, they exceed the friction of the structure where the PI stage is mounted on, so not the full stiffness of the mechanism can be measured. The extra experiment for the stiffness of the base frame resulted in the frame being 7 times more stiff than the measured stiffness of the mechanism.

D. Results

All results of the simulations with corrected dimensions are closer to the experimental results than the simulation results with the optimized dimensions, so this data set is a nice addition to make a better comparison between the results. However, for some results, there still are some differences.

1) Parasitic motion: The results for parasitic motion with the bistable element are very close because the values are in an order of magnitude of 10^{-4}. As stated before in the previous subsection of the discussion on the experiment, it was tried to place the rails that hold the lasers to be as level to the ground as possible. The deviation between the simulated and experimental results might be present because this rail was not level enough. So the results are plotted to relatively different angles, where the simulations would be perfect. For the first $50mm$ of the stroke, the error margin between the mean value derived from experimental data and the results of the simulation with corrected data is within $0.1mm$. For the final $20mm$ the error margin has a maximum of $0.27mm$. For the results without the bistable element, all are within $0.35mm$. The error margin between the mean value derived from experimental data and the results of the simulation with corrected data

is within $0.1mm$. The values of the results of the simulations with corrected dimensions are 1.5 times larger than the results of the simulations with optimized dimensions.

2) Support stiffness: The difference between the experimental results compared to the results of the simulations with optimized dimensions is quite large, the support stiffness is almost 8 times larger. This might be due to fabrication deviations, wrong material properties, or something wrong with the experimental setup. However, with the results of the simulation with corrected dimensions, the results differ by a factor of almost 5 with both experimental results. So now the material properties and dimensions should be more accurate. The overall shape of the results is somewhat similar. The stiffness of the mechanism at the beginning of the stroke is for all results around 1.5 times smaller than the stiffness at the end of the stroke, except for the laser experiment. This 1.5 factor might be present due to the difference in shape of the flexures. As can be seen in Fig. 5, before step two, the shuttle and the second half of the folded leaf flexure have an angle of 45 degrees between them, while after step two the second half of the folded leaf flexure is almost in line with the shuttle. Which would apparently result in a stiffer position. For the flexures, a three-point bending test has been executed to acquire the correct values of the material properties. What might be the case, is that the material properties for these flexures are different than the torsion reinforcement flexures, because these structures have been 3D printed. The torsion reinforcement flexures cannot be tested or experimented on easily, so it might be possible that the deviation is due to this difference in material properties. As discussed in IV-C, the lack of an infinite stiff base frame might also cause the factor 5 difference.

3) Bistability: The results for bistability in the force-displacement graphs of the experiments and simulations are very close. While the results of the experiments and simulation with corrected dimensions follow each other closely, the shape of the stroke backward seems to be more similar to the corrected results, only force difference of one to two Newton. The error margin in results between the optimized dimension and the experiment is within $1N$ for the first $50mm$ of the stroke and within $4N$ for the last part of the stroke. The occurred hysteresis is possible due to the viscosity of the material. This force difference of the hysteresis might also be introduced by the pulley that displaces the mass up and down at the end of the fishing line during the stroke. Creep is also noticeable in the plot; when the shuttle was positioned in its second stable position, there was a force difference at the end of the first stroke and the start of the second. An experiment for friction in the pulley was performed which showed a force difference in the order of magnitude of $0.2N$, which is an order of magnitude lower, so this can be neglected as a main reason for the hysteresis.

E. Case study

When looking at the differences between results with and without bistable elements: the high stiffness and low parasitic motion still hold, while the concept is now bistable and still has a large stroke. This indicates that the proof of concept works.

With the comparison of the experimental results and simulation with the corrected dimensions, there is a small margin of error. This means that when the prototype is made out of titanium, according to Fig. 13, the requirements of the case study will be met. The support stiffness is in the order of magnitude of 10^6 and the parasitic motion is in the order of magnitude of 10^{-6}. This material would have more relaxation, so creep does not occur that fast, which probably removes a big part of the hysteresis.

F. Recommendations

For further research improving the bistable element flexures is recommended. Manufacture the bistable elements out of some sort of metal, so hysteresis and creep do not occur so fast. Then maybe the bistable element can be fixed in place and does not need to be changed after a few experiments. However, take into account that different thicknesses of these flexures alter the bistability of the mechanism. See if for the test setup the rails, to which the lasers are mounted, can be positioned perfectly level, while also making sure the middle of the measuring ranges are aligned correctly. This

way no relative difference between the lasers and the data can be used more efficiently.

V. Conclusion

In this paper, a new design for a bistable linear guide with high support stiffness is investigated and validated with experimental tests. The design is a combination of a flexure-based linear guide and a bistable compliant switch mechanism. It is evaluated and implemented with an FEA, and optimized afterward to acquire a final design. A parametric model was optimized to fulfill the requirements. The optimization goals were maximizing stiffness and minimizing parasitic motion in the direction perpendicular to the axis of the stroke while maintaining bistability. The dimensions of the optimized model were determined during this optimization, so the prototype could be fabricated into a 3D printed model. Experiments on the prototype validate the results from the FEA. The parasitic motion of the prototype was within $1mm$, and its minimum stiffness is at least $10kN/m$ while still having a stroke of $70mm$. These found values are in the same order of magnitude as, and quite close to, the results of the simulations with corrected dimensions. The parasitic motion has an error of margin smaller than $0.1mm$ for the largest part of the stroke, with a maximum of $0.27mm$ in the last part of the stroke. However, the support stiffness had a difference of factor five. The design was indeed still bistable with negative stiffness and a peak and valley in the force-displacement diagram. The results for bistability of the experiments and the simulations with corrected dimensions have an error of margin within $1N$ for the largest part of the stroke, with a maximum of $4N$ in the last part of the stroke. Differences between the linear guide with and without the bistable element are minimal and show that it is still reasonable as a linear guide while maintaining bistability. In general, the results of this work show how to create a bistable linear guide with maintained high support stiffness and low parasitic motion, while still having a large stroke. The case study shows promising potential when the mechanism is made out of the right materials, pure-grade titanium for example. Bistability does not influence the characteristics of the linear guide, so it is a great asset in areas where accuracy in μm or support stiffness in MN/m have to be achieved.

References

[1] Liang X. Shao S and X. Li. “Experimental investigation of particle dispersion in cleanrooms of electronic industry under different area ratios and speeds of fan filter units”. In: *Journal of building engineering* (2021). DOI: 10.1016/J.JOBE.2021.102590.

[2] T. Jiang and K. Jiang. “Numerical analysis of a hydrodynamic air bearing with electromagnetic assistance”. In: *Journal of Engineering Triboligy* 237 (6 2022). DOI: 10.1177/13506501221100617.

[3] S. Ro and J. Park. “A Compact Ultra-precision Air Bearing Stage with 3-DOF Planar Motions Using Electromagnetic Motors”. In: *Journal of precision engineering and manufacturing* 12 (2011), pp. 115–119. DOI: 10.1007/s12541-011-0014-y.

[4] Compliant Mechanism Research Group Brigham Young University. *Compliant mechanisms explained*. Available at https://www.compliantmechanisms.byu.edu/about-compliant-mechanisms.

[5] A. B. Mackay et al. “Metrics for Evaluation and Design of Large-Displacement Linear-Motion Compliant Mechanisms”. In: *Journal of Mechanical Design* 134.1 (2012), p. 011008. DOI: 10.1115/1.4004191.

[6] Shuvam Senapati. *FASCINATING WORLD OF COMPLIANT MECHANISMS*. Available at https://ieee.nitk.ac.in/blog/compliant-mechanisms. 2017.

[7] Solehuddin Shuib, M.I.Z. Ridzwan, and A.H. Kadarman. “Methodology of Compliant Mechanisms and its Current Developments in Applications: A Review”. In: *Compliant Mechanism Applications* (2007). ISSN: 1546-9239. DOI: 10.3844/ajassp.2007.160.167.

[8] Kee Bong Choi and Doo Hyeong Kim. “Monolithic parallel linear compliant mechanism for two axes ultraprecision linear motion”. In: *Review of Scientific Instruments*

77.6 (2006). ISSN: 00346748. DOI: 10.1063/1.2207368.

[9] Larry L. Howell. *Compliant Mechanisms*. John Wiley & Sons, 2001.

[10] CMDE Labs. *Compliant Mechanism: Advantages & Challenges*. Available at https://cmdelabs.medium.com/compliant-mechanism-advantages-challenges-27ff4a0e0566. 2021.

[11] Z. Zhou et al. "A bistable mechanism with linear negative stiffness and large in-plane lateral stiffness: design, modeling and case studies". In: *Mech. Sci* (2020). DOI: 10.5194/ms-11-75-2020.

[12] L. Yan, S. Lu, and P. Liu. "Development of a Fully Compliant Bistable Mechanism Based on Circular Beams with Enhanced Pitch Stiffness". In: *Appl. Sci* (2023). DOI: 10.3390/app13031642.

[13] J. Zhao and Y. Yang. "A Bistable Threshold Accelerometer With Fully Compliant Clamped-Clamped Mechanism". In: *IEEE Sensors Journal* (2010). DOI: 10.1109/JSEN.2010.2042712.

[14] Shannon A. Zirbel et al. "Bistable mechanisms for space applications". In: *PLoS ONE* 11.12 (Dec. 2016). ISSN: 19326203. DOI: 10.1371/journal.pone.0168218.

[15] A. Alqasimi, C. Lusk, and J. Chimento. "Design of a Linear Bistable Compliant Crank–Slider Mechanism". In: *J. Mechanisms Robotics.* (2016). DOI: 10.1115/1.4032509.

[16] D.M. Brouwer J.Rommers M. Naves and J.L. Herder. "A large range spatial linear guide with torsion reinforcement structures". In: *Journal of Mechanics and Robotics* (2021). DOI: 10.1115/1.4052971.

[17] J.-M. Battini and C. Pacoste. "Co-rotational beam elements with warping effects in instability problems". In: *Computer Methods in Applied Mechanics and Engineering* 191.17-18 (2002), pp. 1775–1789.

[18] MakeItFrom. *Polylactic Acid (PLA, Polylactide)*. Available at https://www.makeitfrom.com/material-properties/Polylactic-Acid-PLA-Polylactide. 2020.

4

Conclusion

This report shows a new design for a large-range bistable linear guide with high support stiffness and low parasitic motion is investigated and validated with experimental tests. A literature review was done to find information about linear motion mechanisms making use of compliant mechanism technology. After that, the new design with the desired behavior is obtained, which can be seen in the research paper.

To get insight into the current status of compliant linear guides, a literature review has been done. These mechanisms were divided into different categories, based on what kind of symmetry they hold, and if they move in a straight or approximate straight line. The performance of the mechanisms was evaluated on several criteria. The outcome of the review was that the plane and rotational symmetric designs proved to be the best option for designing compliant linear motion mechanisms. The review also showed that there are no designs that are bistable while still offering high support stiffness, low parasitic motion and a large stroke, which is a research gap in this field.

The goal of the paper is to present a new design that meets these requirements. The design is a combination of a flexure-based linear guide by Rommers and a bistable compliant switch mechanism. It is evaluated, implemented with an FEA, and optimized afterward to acquire a final design. A parametric model was optimized to fulfill the requirements. The optimization goals were maximizing stiffness and minimizing parasitic motion in the direction perpendicular to the axis of the stroke while maintaining bistability. The dimensions of the optimized model were determined during this optimization so that the prototype could be fabricated into a 3D printed model. Experiments on the prototype validate the results from the FEA. The parasitic motion of the prototype was within $1mm$, and its minimum stiffness is at least $10kN/m$ while still having a stroke of $70mm$. These found values are in the same order of magnitude as the simulations with, and quite close to, the results of the simulations with corrected dimensions. The design was still bistable with negative stiffness and a peak and valley in the force-displacement diagram. Differences between the linear guide with and without the bistable element are minimal and show that it is still reliable as a linear guide while maintaining bistability.

The design presented in the paper has been applied to the case study of a tool that concentrically aligns two cylinders, one of which is a magnet. The design variables were optimized such that the mechanism meets the requirements. The tooling shows promising potential when the mechanism is made out of the right materials, pure-grade titanium for example. Bistability does not influence the characteristics of the linear guide, so it is a great asset in areas where accuracy in μm or support stiffness in MN/m have to be achieved.

Appendix A - Concept generation

For the design of a bistable linear guide, different concepts on linear guiding have been reviewed, the same holds for bistable mechanisms. For the concept generation different combinations of linear guides and bistable mechanisms have been considered. Each of these will be explained in this section.

A.1. Concept 1

The first concept is a variation on a conventional compliant switch mechanism, a bistable compliant mechanism. However, this is a 3D design, so it encloses the shuttle from three sides. Multiple bistable beams can be put in place to counter the warp a bistable mechanism might have. Because of the symmetry the design would have minimal parasitic motion and support stiffness would be quite high relative to its size.

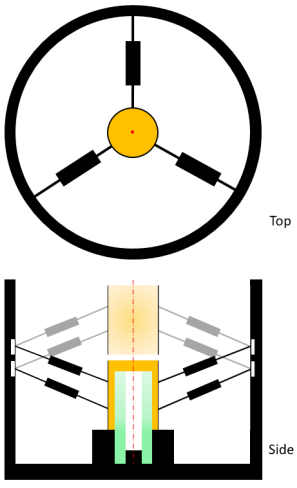

Figure A.1: Concept 1

A.2. Concept 2

The second concept is based on the same bistable compliant mechanism. However, in this design, extra springs have been put in place to compensate for the warp of the shuttle. This 2D design could be made quite compact, but the question would be if the support stiffness would drop significantly by the addition of these springs.

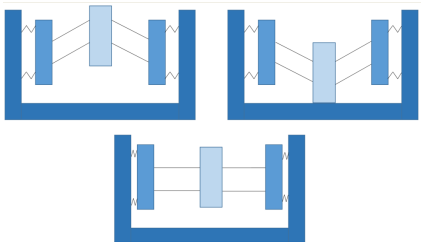

Figure A.2: Concept 2

A.3. Concept 3

The third concept is based on the linear guides that are mainly used in MEMS. The design would be scalable, so it would be able to reach the required stroke. However, this would mean the entire design would become quite large. Another challenge would be to make these bistable. Their parasitic motion and support stiffness are relatively high compared to their size.

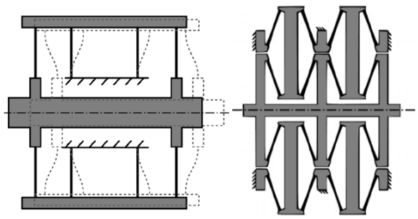

Figure A.3: Inspiration for concept 3

A.4. Concept 4

This design uses the design of Rommers as a starting point. It offers high support stiffness and low parasitic motion while making a large stroke. The design is quite small relative to its stroke. The challenge here would be to make it bistable. By combining the basic bistable compliant mechanism as has been mentioned previously and this linear guide, the requirements of this paper could be met.

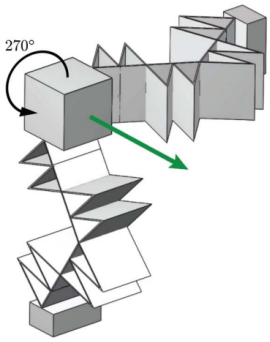

Figure A.4: Inspiration for concept 4

A.5. Final design

After considering the concepts, concept 4 has been chosen to work with. It showed most promise for combining mechanisms, while the others had more difficult challenges to tackle or other uncertainties. Concept 1 would be very hard to manufacture and test with a prototype. Another issue is that the support stiffness would probably be too low as well. Option 2 would be very interesting to see to be brought to life. But here the support stiffness would be an issue as well, because of the springs in series the stiffness will drop significantly. Concept 3 will be probably too big if it needs to make the required stroke. On top of that, to make it bistable would also be a big challenge. In the end, option 4 seems to

be the best, because it has the best starting point to work on. The principle is simple while still being very efficient. The design has been explained and evaluated in the paper.

B

Appendix B - Additional experiments

B.1. E-modulus

One of the factors that could realize this difference is the wrong chosen material properties, an average of found values was used, but because of the range of found values there is some uncertainty. That is why a three-point bending test has been performed on the 3D printed bistable flexures with the torque en tensile sensors of Zwick Roell KAF-TC. Now the correct E-modulus and G-modulus can be calculated. Multiple tests per sample have been done, with 3 samples per color, so both the properties for the grey and black flexures can be acquired. The experiments resulted in force-displacement graphs, from which the slope could be calculated. Inserting that in the formula for the E-modulus: $E = (slope * L^3)/(48I)$ where the moment of inertia I for both colors is different, with I being $I = (bh^3)/12$. Resulting in an E-modulus of 3D printed parts: $E(blackparts) = 2.418GPa$ and $E(greyparts) = 2.592GPa$.

B.2. Force difference in bistability plot

An experiment of bistability without the model has been performed, to check why there is a force difference during the stroke back and forth. As visible in Figure B.1, the force difference between the pulley and mass is around $0.2N$, which means it has no significant impact on the results.

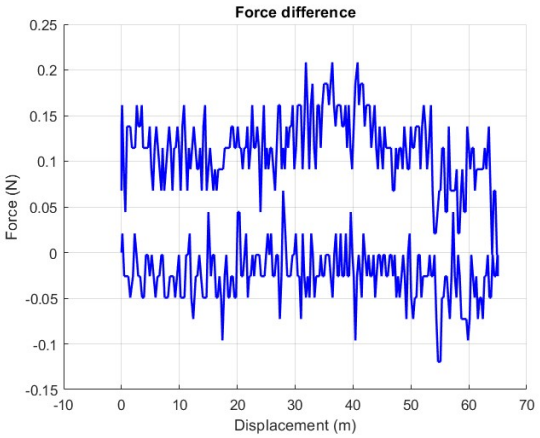

Figure B.1: Force difference during the stroke with only a mass and pulley.

C

Appendix C - Additional results

C.1. Stress results

In figure C.1 and C.2 the von Mises stress plots can be seen of the design of Rommers, which the design in the paper is based on. The stress build-up is maximum around the connection of the torsion reinforced flexure and the base.

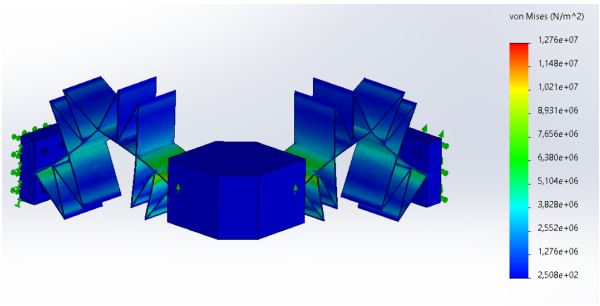

Figure C.1: Von Mises stress when applying a displacement of 25mm upwards.

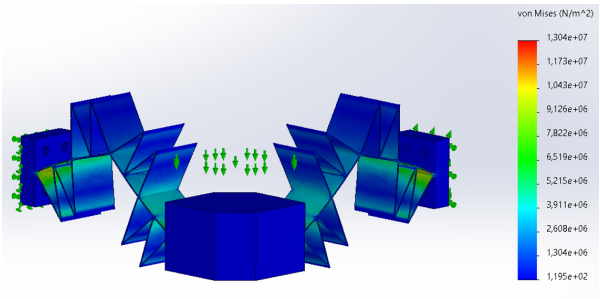

Figure C.2: Von Mises stress when applying a displacement of 25mm downwards.

Keep in mind that these simulations were done without the bistable element in place.

D

Appendix D - Code

D.1. Objective function

Main code for the objective function:

```
function objective = Param_opt_3runs(variables)

TBB = variables(1);
V   = variables(2);
LB  = variables(3);
HBB = variables(4);
TF  = variables(5);
HF  = variables(6);

close all
% clear all
par.nTimestep   = 100;
par.nIter       = 100;
par.conv        = 1e-6;
par.plots       = 'off';
par.getKend     = 0;
par.step = 'off'
addpath '..\core'

%% Model
% generation of coordinates and connectivities

%Parameters

%elements
e_s = 20;        %elements-side
e_f = 10;        %elements-fin
e_b2= 8;         %elements-base2
e_b = e_b2*2-1; %elements-base

%angles
alpha   = 60;
beta    = 44.48;
gamma   = 74.48;
delta   = 45;
epsilon = 15.44;

%moving module
S   = 37.573e-3;  %side moving module
S_b = 36.22e-3;   %side base moving module
```

```
TMM = 40e-3;       %thickness moving module
HMM = 40e-3;       %height moving module
L   = 80e-3;       %leaf flexure
F   = 40e-3;       %fin

%displacements
X_stroke  = 70e-3;
X_initial = 0.5*X_stroke;

%Connections

x=[linspace(0,L*cosd(alpha),e_s)...
   linspace(L*cosd(alpha),0,e_s)...
   linspace(0,0,e_b2)...
   linspace(0,0,e_b2)...
   linspace(0,L*cosd(alpha),e_s)...
   linspace(L*cosd(alpha),0,e_s)...
   linspace(0,-F*sind(beta),e_f)...
   linspace(-F*sind(beta),0.25*L*cosd(alpha),e_f)...
   linspace(0.25*L*cosd(alpha),0.25*L*cosd(alpha)-F*sind(beta),e_f)...
   linspace(0.25*L*cosd(alpha)-F*sind(beta),0.5*L*cosd(alpha),e_f)...
   linspace(0.5*L*cosd(alpha),0.5*L*cosd(alpha)+F*sind(gamma),e_f)...
   linspace(0.5*L*cosd(alpha)+F*sind(gamma),0.75*L*cosd(alpha),e_f)...
   linspace(0.75*L*cosd(alpha),0.75*L*cosd(alpha)+F*sind(gamma),e_f)...
   linspace(0.75*L*cosd(alpha)+F*sind(gamma),L*cosd(alpha),e_f)...
    linspace(L*cosd(alpha),0.75*L*cosd(alpha)+F*sind(gamma),e_f)...
   linspace(0.75*L*cosd(alpha)+F*sind(gamma),0.75*L*cosd(alpha),e_f)...
   linspace(0.75*L*cosd(alpha),0.5*L*cosd(alpha)+F*sind(gamma),e_f)...
   linspace(0.5*L*cosd(alpha)+F*sind(gamma),0.5*L*cosd(alpha),e_f)...
   linspace(0.5*L*cosd(alpha),0.25*L*cosd(alpha)-F*sind(beta),e_f)...
   linspace(0.25*L*cosd(alpha)-F*sind(beta),0.25*L*cosd(alpha),e_f)...
   linspace(0.25*L*cosd(alpha),-F*sind(beta),e_f)...
   linspace(-F*sind(beta),0,e_f)...
    linspace(0,-F*sind(beta),e_f)...
   linspace(-F*sind(beta),0.25*L*cosd(alpha),e_f)...
   linspace(0.25*L*cosd(alpha),0.25*L*cosd(alpha)-F*sind(beta),e_f)...
   linspace(0.25*L*cosd(alpha)-F*sind(beta),0.5*L*cosd(alpha),e_f)...
   linspace(0.5*L*cosd(alpha),0.5*L*cosd(alpha)+F*sind(gamma),e_f)...
   linspace(0.5*L*cosd(alpha)+F*sind(gamma),0.75*L*cosd(alpha),e_f)...
   linspace(0.75*L*cosd(alpha),0.75*L*cosd(alpha)+F*sind(gamma),e_f)...
   linspace(0.75*L*cosd(alpha)+F*sind(gamma),L*cosd(alpha),e_f)...
    linspace(L*cosd(alpha),0.75*L*cosd(alpha)+F*sind(gamma),e_f)...
   linspace(0.75*L*cosd(alpha)+F*sind(gamma),0.75*L*cosd(alpha),e_f)...
   linspace(0.75*L*cosd(alpha),0.5*L*cosd(alpha)+F*sind(gamma),e_f)...
   linspace(0.5*L*cosd(alpha)+F*sind(gamma),0.5*L*cosd(alpha),e_f)...
   linspace(0.5*L*cosd(alpha),0.25*L*cosd(alpha)-F*sind(beta),e_f)...
   linspace(0.25*L*cosd(alpha)-F*sind(beta),0.25*L*cosd(alpha),e_f)...
   linspace(0.25*L*cosd(alpha),-F*sind(beta),e_f)...
   linspace(-F*sind(beta),0,e_f)...
   linspace(0,0,e_f)...
   linspace(0,0,e_s)]';
x([e_s,2*e_s,2*e_s+e_b2,2*e_s+2*e_b2,3*e_s+2*e_b2+1,4*e_s+2*e_b2+1, ...
    4*e_s+2*e_b2+e_f+1,4*e_s+2*e_b2+2*e_f+1,4*e_s+2*e_b2+3*e_f+1, ...
    4*e_s+2*e_b2+4*e_f,4*e_s+2*e_b2+5*e_f,4*e_s+2*e_b2+6*e_f, ...
    4*e_s+2*e_b2+7*e_f,4*e_s+2*e_b2+8*e_f,4*e_s+2*e_b2+8*e_f+1, ...
    4*e_s+2*e_b2+9*e_f+1,4*e_s+2*e_b2+10*e_f+1,4*e_s+2*e_b2+11*e_f+1, ...
    4*e_s+2*e_b2+12*e_f+1,4*e_s+2*e_b2+13*e_f+1,4*e_s+2*e_b2+14*e_f+1, ...
    4*e_s+2*e_b2+15*e_f+1,4*e_s+2*e_b2+16*e_f,4*e_s+2*e_b2+16*e_f+1, ...
    4*e_s+2*e_b2+16*e_f+1,4*e_s+2*e_b2+17*e_f+1,4*e_s+2*e_b2+18*e_f+1, ...
    4*e_s+2*e_b2+19*e_f+1,4*e_s+2*e_b2+20*e_f+1,4*e_s+2*e_b2+21*e_f+1, ...
    4*e_s+2*e_b2+22*e_f+1,4*e_s+2*e_b2+23*e_f+1,4*e_s+2*e_b2+24*e_f, ...
```

```
    4*e_s+2*e_b2+24*e_f+1,4*e_s+2*e_b2+25*e_f+1,4*e_s+2*e_b2+26*e_f+1, ...
    4*e_s+2*e_b2+27*e_f+1,4*e_s+2*e_b2+28*e_f+1,4*e_s+2*e_b2+29*e_f+1, ...
    4*e_s+2*e_b2+30*e_f+1,4*e_s+2*e_b2+31*e_f+1,4*e_s+2*e_b2+32*e_f, ...
    4*e_s+2*e_b2+32*e_f+1,4*e_s+2*e_b2+33*e_f+1])=[];

y=[linspace(0,L*sind(alpha),e_s)...
   linspace(L*sind(alpha),2*L*sind(alpha),e_s)...
   linspace(2*L*sind(alpha),2*L*sind(alpha)+S*cosd(epsilon),e_b2)...
   linspace(2*L*sind(alpha)+S*cosd(epsilon),2*L*sind(alpha)+ ...
   S*sind(epsilon)+S*cosd(epsilon),e_b2)...
   linspace(2*L*sind(alpha)+S*sind(epsilon)+S*cosd(epsilon), ...
   2*L*sind(alpha)+S*sind(epsilon)+S*cosd(epsilon),e_s)...
   linspace(2*L*sind(alpha)+S*sind(epsilon)+S*cosd(epsilon), ...
   2*L*sind(alpha)+S*sind(epsilon)+S*cosd(epsilon),e_s)...
   linspace(0,F*cosd(beta),e_f)...
   linspace(F*cosd(beta),0.25*L*sind(alpha),e_f)...
   linspace(0.25*L*sind(alpha),0.25*L*sind(alpha)+F*cosd(beta),e_f)...
   linspace(0.25*L*sind(alpha)+F*cosd(beta),0.5*L*sind(alpha),e_f)...
   linspace(0.5*L*sind(alpha),0.5*L*sind(alpha)-F*cosd(gamma),e_f)...
   linspace(0.5*L*sind(alpha)-F*cosd(gamma),0.75*L*sind(alpha),e_f)...
   linspace(0.75*L*sind(alpha),0.75*L*sind(alpha)-F*cosd(gamma),e_f)...
   linspace(0.75*L*sind(alpha)-F*cosd(gamma),L*sind(alpha),e_f)...
    linspace(L*sind(alpha),L*sind(alpha)+F*sind(beta),e_f)...
   linspace(L*sind(alpha)+F*sind(beta),1.25*L*sind(alpha),e_f)...
   linspace(1.25*L*sind(alpha),1.25*L*sind(alpha)+F*sind(beta),e_f)...
   linspace(1.25*L*sind(alpha)+F*sind(beta),1.5*L*sind(alpha),e_f)...
   linspace(1.5*L*sind(alpha),1.5*L*sind(alpha)-F*cosd(gamma),e_f)...
   linspace(1.5*L*sind(alpha)-F*cosd(gamma),1.75*L*sind(alpha),e_f)...
   linspace(1.75*L*sind(alpha),1.75*L*sind(alpha)-F*cosd(gamma),e_f)...
   linspace(1.75*L*sind(alpha)-F*cosd(gamma),2*L*sind(alpha),e_f)...
    linspace(2*L*sind(alpha)+S*cosd(epsilon)+S*sind(epsilon),2*L*sind(alpha)+ ...
    S*cosd(epsilon)+S*sind(epsilon),16*e_f)...
   linspace(2*L*sind(alpha)+S*cosd(epsilon),2*L*sind(alpha)+S*cosd(epsilon)- ...
   S_b*cosd(delta),e_f)...
   linspace(2*L*sind(alpha)+S*cosd(epsilon)-S_b*cosd(delta),2*L*sind(alpha)+ ...
   S*cosd(epsilon)-S_b*cosd(delta)-LB*cosd(delta),e_s)]';
y([e_s,2*e_s,2*e_s+e_b2,2*e_s+2*e_b2,3*e_s+2*e_b2+1,4*e_s+2*e_b2+1, ...
    4*e_s+2*e_b2+e_f+1,4*e_s+2*e_b2+2*e_f+1,4*e_s+2*e_b2+3*e_f+1, ...
    4*e_s+2*e_b2+4*e_f,4*e_s+2*e_b2+5*e_f,4*e_s+2*e_b2+6*e_f, ...
    4*e_s+2*e_b2+7*e_f,4*e_s+2*e_b2+8*e_f,4*e_s+2*e_b2+8*e_f+1, ...
    4*e_s+2*e_b2+9*e_f+1,4*e_s+2*e_b2+10*e_f+1,4*e_s+2*e_b2+11*e_f+1, ...
    4*e_s+2*e_b2+12*e_f+1,4*e_s+2*e_b2+13*e_f+1,4*e_s+2*e_b2+14*e_f+1, ...
    4*e_s+2*e_b2+15*e_f+1,4*e_s+2*e_b2+16*e_f,4*e_s+2*e_b2+16*e_f+1, ...
    4*e_s+2*e_b2+16*e_f+1,4*e_s+2*e_b2+17*e_f+1,4*e_s+2*e_b2+18*e_f+1, ...
    4*e_s+2*e_b2+19*e_f+1,4*e_s+2*e_b2+20*e_f+1,4*e_s+2*e_b2+21*e_f+1, ...
    4*e_s+2*e_b2+22*e_f+1,4*e_s+2*e_b2+23*e_f+1,4*e_s+2*e_b2+24*e_f, ...
    4*e_s+2*e_b2+24*e_f+1,4*e_s+2*e_b2+25*e_f+1,4*e_s+2*e_b2+26*e_f+1, ...
    4*e_s+2*e_b2+27*e_f+1,4*e_s+2*e_b2+28*e_f+1,4*e_s+2*e_b2+29*e_f+1, ...
    4*e_s+2*e_b2+30*e_f+1,4*e_s+2*e_b2+31*e_f+1,4*e_s+2*e_b2+32*e_f, ...
    4*e_s+2*e_b2+32*e_f+1,4*e_s+2*e_b2+33*e_f+1])=[];

z=[linspace(0,0,e_s)...
  linspace(0,0,e_s)...
  linspace(0,S*sind(epsilon),e_b2)...
  linspace(S*sind(epsilon),S*sind(epsilon)+S*cosd(epsilon),e_b2)...
  linspace(S*sind(epsilon)+S*cosd(epsilon),S*sind(epsilon)+S*cosd(epsilon)+ ...
  L*sind(alpha),e_s)...
  linspace(S*sind(epsilon)+S*cosd(epsilon)+L*sind(alpha),S*sind(epsilon)+ ...
  S*cosd(epsilon)+2*L*sind(alpha),e_s)...
  linspace(0,0,e_f)...
  linspace(0,0,e_f)...
```

```
  linspace(0,0,e_f)...
  linspace(0,0,e_f)...
  linspace(0,0,e_f)...
  linspace(0,0,e_f)...
  linspace(0,0,e_f)...
  linspace(0,0,e_f)...
  linspace(0,0,8*e_f)...
   linspace(S*sind(epsilon)+S*cosd(epsilon),S*sind(epsilon)+S*cosd(epsilon)+ ...
   F*cosd(beta),e_f)...
  linspace(S*sind(epsilon)+S*cosd(epsilon)+F*cosd(beta),S*sind(epsilon)+ ...
  S*cosd(epsilon)+ 0.25*L*sind(alpha),e_f)...
  linspace(S*sind(epsilon)+S*cosd(epsilon)+0.25*L*sind(alpha),S*sind(epsilon)+ ...
  S*cosd(epsilon)+0.25*L*sind(alpha)+F*cosd(beta),e_f)...
  linspace(S*sind(epsilon)+S*cosd(epsilon)+0.25*L*sind(alpha)+F*cosd(beta), ...
  S*sind(epsilon)+S*cosd(epsilon)+0.5*L*sind(alpha),e_f)...
  linspace(S*sind(epsilon)+S*cosd(epsilon)+0.5*L*sind(alpha),S*sind(epsilon)+ ...
  S*cosd(epsilon)+0.5*L*sind(alpha)-F*cosd(gamma),e_f)...
  linspace(S*sind(epsilon)+S*cosd(epsilon)+0.5*L*sind(alpha)-F*cosd(gamma), ...
  S*sind(epsilon)+S*cosd(epsilon)+0.75*L*sind(alpha),e_f)...
  linspace(S*sind(epsilon)+S*cosd(epsilon)+0.75*L*sind(alpha),S*sind(epsilon)+ ...
  S*cosd(epsilon)+0.75*L*sind(alpha)-F*cosd(gamma),e_f)...
  linspace(S*sind(epsilon)+S*cosd(epsilon)+0.75*L*sind(alpha)-F*cosd(gamma), ...
  S*sind(epsilon)+S*cosd(epsilon)+L*sind(alpha),e_f)...
   linspace(S*sind(epsilon)+S*cosd(epsilon)+L*sind(alpha),S*sind(epsilon)+ ...
   S*cosd(epsilon)+L*sind(alpha)+F*sind(beta),e_f)...
  linspace(S*sind(epsilon)+S*cosd(epsilon)+L*sind(alpha)+F*sind(beta), ...
  S*sind(epsilon)+S*cosd(epsilon)+1.25*L*sind(alpha),e_f)...
  linspace(S*sind(epsilon)+S*cosd(epsilon)+1.25*L*sind(alpha),S*sind(epsilon)+ ...
  S*cosd(epsilon)+1.25*L*sind(alpha)+F*sind(beta),e_f)...
  linspace(S*sind(epsilon)+S*cosd(epsilon)+1.25*L*sind(alpha)+F*sind(beta), ...
  S*sind(epsilon)+S*cosd(epsilon)+1.5*L*sind(alpha),e_f)...
  linspace(S*sind(epsilon)+S*cosd(epsilon)+1.5*L*sind(alpha),S*sind(epsilon)+ ...
  S*cosd(epsilon)+1.5*L*sind(alpha)-F*cosd(gamma),e_f)...
  linspace(S*sind(epsilon)+S*cosd(epsilon)+1.5*L*sind(alpha)-F*cosd(gamma), ...
  S*sind(epsilon)+S*cosd(epsilon)+1.75*L*sind(alpha),e_f)...
  linspace(S*sind(epsilon)+S*cosd(epsilon)+1.75*L*sind(alpha),S*sind(epsilon)+ ...
  S*cosd(epsilon)+1.75*L*sind(alpha)-F*cosd(gamma),e_f)...
  linspace(S*sind(epsilon)+S*cosd(epsilon)+1.75*L*sind(alpha)-F*cosd(gamma), ...
  S*sind(epsilon)+S*cosd(epsilon)+2*L*sind(alpha),e_f)...
  linspace(S*sind(epsilon),S*sind(epsilon)+S_b*sind(delta),e_f)...
  linspace(S*sind(epsilon)+S_b*sind(delta),S*sind(epsilon)+S_b*sind(delta)+ ...
  LB*sind(delta),e_s)]';
z([e_s,2*e_s,2*e_s+e_b2,2*e_s+2*e_b2,3*e_s+2*e_b2+1,4*e_s+2*e_b2+1, ...
    4*e_s+2*e_b2+e_f+1,4*e_s+2*e_b2+2*e_f+1,4*e_s+2*e_b2+3*e_f+1, ...
    4*e_s+2*e_b2+4*e_f,4*e_s+2*e_b2+5*e_f,4*e_s+2*e_b2+6*e_f, ...
    4*e_s+2*e_b2+7*e_f,4*e_s+2*e_b2+8*e_f,4*e_s+2*e_b2+8*e_f+1, ...
    4*e_s+2*e_b2+9*e_f+1,4*e_s+2*e_b2+10*e_f+1,4*e_s+2*e_b2+11*e_f+1, ...
    4*e_s+2*e_b2+12*e_f+1,4*e_s+2*e_b2+13*e_f+1,4*e_s+2*e_b2+14*e_f+1, ...
    4*e_s+2*e_b2+15*e_f+1,4*e_s+2*e_b2+16*e_f,4*e_s+2*e_b2+16*e_f+1, ...
    4*e_s+2*e_b2+16*e_f+1,4*e_s+2*e_b2+17*e_f+1,4*e_s+2*e_b2+18*e_f+1, ...
    4*e_s+2*e_b2+19*e_f+1,4*e_s+2*e_b2+20*e_f+1,4*e_s+2*e_b2+21*e_f+1, ...
    4*e_s+2*e_b2+22*e_f+1,4*e_s+2*e_b2+23*e_f+1,4*e_s+2*e_b2+24*e_f, ...
    4*e_s+2*e_b2+24*e_f+1,4*e_s+2*e_b2+25*e_f+1,4*e_s+2*e_b2+26*e_f+1, ...
    4*e_s+2*e_b2+27*e_f+1,4*e_s+2*e_b2+28*e_f+1,4*e_s+2*e_b2+29*e_f+1, ...
    4*e_s+2*e_b2+30*e_f+1,4*e_s+2*e_b2+31*e_f+1,4*e_s+2*e_b2+32*e_f, ...
    4*e_s+2*e_b2+32*e_f+1,4*e_s+2*e_b2+33*e_f+1])=[];



nbeam = numel(x);
```

```
m.X = [x,y,z,zeros(3,nbeam)'];
m.elementNodes= [1:2*e_s-2   2*e_s-1:2*e_s+e_b-3   2*e_s+e_b-2:4*e_s+e_b-5
    1   4*e_s+e_b-3:4*e_s+e_b+8*e_f-14   4*e_s+e_b+8*e_f-13 0.25*e_s 0.5*e_s
    0.75*e_s  e_s  4*e_s+e_b+8*e_f-12:4*e_s+e_b+16*e_f-23 4*e_s+e_b+16*e_f-22
    1.25*e_s    1.5*e_s    1.75*e_s   2*e_s+e_b-2
        4*e_s+e_b+16*e_f-21:4*e_s+e_b+24*e_f-32
    4*e_s+e_b+24*e_f-31  4*e_s+e_b+18*e_f-24   4*e_s+e_b+20*e_f-26
    4*e_s+e_b+22*e_f-28   e_b+3*e_s-3    4*e_s+e_b+24*e_f-30:4*e_s+e_b+32*e_f-41
    4*e_s+e_b+32*e_f-40   4*e_s+e_b+28*e_f-35   4*e_s+e_b+30*e_f-37
    2*e_s+e_b-9   4*e_s+e_b+32*e_f-39:4*e_s+e_b+33*e_f-42    4*e_s+e_b+33*e_f-41
    4*e_s+e_b+33*e_f-40:5*e_s+e_b+33*e_f-43     ;       2:2*e_s-1
        2*e_s:2*e_s+e_b-2
    2*e_s+e_b-1:4*e_s+e_b-4     4*e_s+e_b-3    4*e_s+e_b-2:4*e_s+e_b+8*e_f-13
    e_s    4*e_s+e_b+2*e_f-6      4*e_s+e_b+4*e_f-8      4*e_s+e_b+6*e_f-10
    4*e_s+e_b+8*e_f-12  4*e_s+e_b+8*e_f-11:4*e_s+e_b+16*e_f-22     2*e_s-1
    4*e_s+e_b+10*e_f-15    4*e_s+e_b+12*e_f-17    4*e_s+e_b+14*e_f-19
    4*e_s+e_b+16*e_f-21   4*e_s+e_b+16*e_f-20:4*e_s+e_b+24*e_f-31   e_b+3*e_s-3
    e_b+2.25*e_s-2  e_b+2.5*e_s-2  e_b+2.75*e_s-2  4*e_s+e_b+24*e_f-30
    4*e_s+e_b+24*e_f-29:4*e_s+e_b+32*e_f-40   e_b+4*e_s-4  e_b+3.5*e_s-3
    e_b+3.75*e_s-3    4*e_s+e_b+32*e_f-39
        4*e_s+e_b+32*e_f-38:4*e_s+e_b+33*e_f-41
    4*e_s+e_b+33*e_f-40    4*e_s+e_b+33*e_f-39:5*e_s+e_b+33*e_f-42]'     ;
m.numberNodes       = size(m.X,1);
m.numberElements    = size(m.elementNodes,1);
m.eqn               = 6*m.numberNodes;
m.x                 = reshape(m.X',m.eqn,1) ;


%PLA
m.E         = 3.50e9 * ones(1,m.numberElements); %youngs modulus
m.G         = 2.4e9 * ones(1,m.numberElements);  %shear modulus

H    = TF * ones(1,m.numberElements); %thickness flexures
H(2*e_s-1:2*e_s+e_b-3) =                    TMM; % moving module
H(4*e_s+e_b+33*e_f-35:4*e_s+e_b+34*e_f-37) = TMM; % moving module
H(4*e_s+e_b+34*e_f-36:5*e_s+e_b+34*e_f-38) = TBB; % bistable beam

W    = HF * ones(1,m.numberElements); %height flexures
W(2*e_s-1:2*e_s+e_b-3) =                    HMM; % moving module
W(4*e_s+e_b+33*e_f-35:4*e_s+e_b+34*e_f-37) = HMM; % moving module
W(4*e_s+e_b+34*e_f-36:5*e_s+e_b+34*e_f-38) = HBB; % bistable beam

m = DefineCrossSection(m,'rectangle',H,W);

%%Use this for a single orientation point
CSO = [ 100 0 0]';   % cross section orientation.
m.GuideCurve = repmat(CSO,1,m.numberElements);
m.guidecurve = reshape(m.GuideCurve,3*m.numberElements,1) ;

%% core

for e = 1:m.numberElements

x21=(m.X(m.elementNodes(e,2),1:3)'-m.X(m.elementNodes(e,1),1:3)');
e01     = (x21)/norm(x21);
%     e03star = veccross(e01,[0.00001 0.000001 1]');
e03star = cross(e01, m.guidecurve(3*(m.elementNodes(e,1)-1)+[1:3]) -
    m.X(m.elementNodes(e,1),1:3)');
e03     = e03star/norm(e03star);
e02     = cross(e03,e01);
Ro      = [e01 e02 e03];       % voor eqn 4.28
```

```
281
282 m.tr1(:,:,m.elementNodes(e,1))         = eye(3)*Ro;
283 m.tr2(:,:,m.elementNodes(e,1))         = eye(3)*Ro;
284 end
285
286 m.tr1(:,:,m.numberElements)          = eye(3)*Ro;
287 m.tr2(:,:,m.numberElements)          = eye(3)*Ro;
288
289 m.Rg1                = repmat(eye(3),1,1,m.numberElements);
290 m.Rg2                = repmat(eye(3),1,1,m.numberElements);
291
292 m.D                  = zeros(6,m.numberNodes)';
293 m.d                  = zeros(m.eqn,1);
294
295
296 % plotBeams(m,'r')
297 grid on
298
299     try
300
301 %% BOUNDARY CONDITIONS on begin- and endpoint
302 % 1st run
303
304 pointconstraints=zeros(6,m.numberNodes); %creates a 6 by N array with zeros
305 pointconstraints([1 2 3 4 5 6],1) = 1;                    %base flexure 1
306 % pointconstraints(1,2*e_s+e_b-9) = 1;                    %middle moving module
307 pointconstraints([1 2 3 4 5 6],4*e_s+e_b-4) = 1;         %base flexure 2
308 pointconstraints([1 2 3 4 5 6],5*e_s+e_b+33*e_f-42) = 1; %base bistable element
309
310 dofs.bc = find(pointconstraints)';
311 dofs.dp = zeros(sum(pointconstraints,'all'),1);
312 activeconstraints = [14,15];
313 dofs.dp(activeconstraints) = [V*cosd(delta),-V*cosd(delta)]; %preload displacement
314
315 Fe  = zeros(m.eqn,1);%geleidelijke kracht toepassen
316 PreFe  = zeros(m.eqn,1); %instant kracht
317
318 dofs.all    = (1:m.eqn)';
319 %dofs.bc     = bc(~isnan([dofs.dp]));
320 %dofs.dp     = dofs.dp(~isnan([dofs.dp]));
321 dofs.R      =
        sparse(1:length(dofs.bc),[dofs.bc],1+0*dofs.bc,length(dofs.bc),m.eqn);
322
323 [history, m] = solveNONLINstaticCOR(m,dofs,par,Fe,PreFe);
324  % plotBeams(m,'b')
325
326  def='def';
327  % PlotBeamsCrossSections(m,par,def)
328
329 %% 2nd run
330
331 pointconstraints=zeros(6,m.numberNodes); %creates a 6 by N array with zeros
332 pointconstraints([1 2 3 4 5 6],1) = 1;                    %base flexure 1
333 pointconstraints(1,2*e_s+e_b-9) = 1;                      %middle moving module
334 pointconstraints([1 2 3 4 5 6],4*e_s+e_b-4) = 1;         %base flexure 2
335 pointconstraints([1 2 3 4 5 6],5*e_s+e_b+33*e_f-42) = 1; %base bistable element
336
337 dofs.bc = find(pointconstraints)';
338 dofs.dp = zeros(sum(pointconstraints,'all'),1);
339 activeconstraints = [7];
340 dofs.dp(activeconstraints) = X_stroke; %displacement of moving module
```

```
341
342 Fe  = zeros(m.eqn,1);%geleidelijke kracht toepassen
343 PreFe  = zeros(m.eqn,1); %instant kracht
344 % PreFe((2*e_s+e_b-10)*6+2) = 5;     % N     y (positief)
345 % PreFe((2*e_s+e_b-10)*6+3) = -5;    % N     z (negatief)
346
347 dofs.all    = (1:m.eqn)';
348 %dofs.bc     = bc(~isnan([dofs.dp]));
349 %dofs.dp     = dofs.dp(~isnan([dofs.dp]));
350 dofs.R      =
    sparse(1:length(dofs.bc),[dofs.bc],1+0*dofs.bc,length(dofs.bc),m.eqn);
351
352
353 [history2, m2] = solveNONLINstaticCOR(m,dofs,par,Fe,PreFe);
354 % plotBeams(m2,'b')
355
356 def='def';
357 % PlotBeamsCrossSections(m,par,def)
358
359 %% 3rd run
360
361 pointconstraints=zeros(6,m.numberNodes); %creates a 6 by N array with zeros
362 pointconstraints([1 2 3 4 5 6],1) = 1;                  %base flexure 1
363 pointconstraints(1,2*e_s+e_b-9) = 1;                    %middle moving module
364 pointconstraints([1 2 3 4 5 6],4*e_s+e_b-4) = 1;        %base flexure 2
365 pointconstraints([1 2 3 4 5 6],5*e_s+e_b+33*e_f-42) = 1; %base bistable element
366
367 dofs.bc = find(pointconstraints)';
368 dofs.dp = zeros(sum(pointconstraints,'all'),1);
369 activeconstraints = [7];
370 dofs.dp(activeconstraints) = X_stroke; %displacement of moving module
371
372 Fe  = zeros(m.eqn,1);%geleidelijke kracht toepassen
373 PreFe  = zeros(m.eqn,1); %instant kracht
374 PreFe((2*e_s+e_b-10)*6+2) = 5;     % N     y (positief)
375 % PreFe((2*e_s+e_b-10)*6+3) = -5;    % N     z (negatief)
376
377 dofs.all    = (1:m.eqn)';
378 %dofs.bc     = bc(~isnan([dofs.dp]));
379 %dofs.dp     = dofs.dp(~isnan([dofs.dp]));
380 dofs.R      =
    sparse(1:length(dofs.bc),[dofs.bc],1+0*dofs.bc,length(dofs.bc),m.eqn);
381
382
383 [history3, m3] = solveNONLINstaticCOR(m,dofs,par,Fe,PreFe);
384 % plotBeams(m2,'b')
385
386 def='def';
387 % PlotBeamsCrossSections(m,par,def)
388
389 %% Objective function
390
391 %make a vector of the positions of x
392 x_positions = zeros(par.nTimestep, 1);
393 for X = 1:par.nTimestep
394     x_positions(X) = history2(X).m.D(2*e_s+e_b-9, 1);
395 end
396
397 %make a vector of the forces on x
398 RF_x_positions = zeros(par.nTimestep, 1);
399 for X = 1:par.nTimestep
```

```
    RF_x_positions(X) = history2(X).RF(7);
end

figure
plot(x_positions,RF_x_positions);
title('Force Displacement plot')
xlabel('Displacement (m)' )
ylabel('Force (N)' )
hold on
grid on


%base position MMM(y,z), after positioning into bistable modus
y_MMM= history(par.nTimestep).m.X(2*e_s+e_b-9,2)+
history(par.nTimestep).m.D(2*e_s+e_b-9,2);
z_MMM= history(par.nTimestep).m.X(2*e_s+e_b-9,3)+
history(par.nTimestep).m.D(2*e_s+e_b-9,3);

%initial positions MMM(y,z) during stroke without preforce
y_MMM = zeros(par.nTimestep, 1);
for X = 1:par.nTimestep
    y_MMM(X) = history2(X).m.X(2*e_s+e_b-9,2)+history2(X).m.D(2*e_s+e_b-9,2);
end

z_MMM = zeros(par.nTimestep, 1);
for X = 1:par.nTimestep
    z_MMM(X) = history2(X).m.X(2*e_s+e_b-9,3)+history2(X).m.D(2*e_s+e_b-9,3);
end

%new coordinates MMM(y,z) during stroke with preforce
y_MMM_new = zeros(par.nTimestep, 1);
for X = 1:par.nTimestep
    y_MMM_new(X) = history3(X).m.X(2*e_s+e_b-9,2)+history3(X).m.D(2*e_s+e_b-9,2);
end

z_MMM_new = zeros(par.nTimestep, 1);
for X = 1:par.nTimestep
    z_MMM_new(X) = history3(X).m.X(2*e_s+e_b-9,3)+history3(X).m.D(2*e_s+e_b-9,3);
end

%displacement vectors
initial_MMM   = [y_MMM,z_MMM];
new_MMM       = [y_MMM_new,z_MMM_new];
parasitic_MMM = new_MMM - initial_MMM;


%stiffness dF/dy at MMM(y) & dF/dz at MMM(z)
y_stiffness = PreFe((2*e_s+e_b-10)*6+2) ./ parasitic_MMM(:,1);
z_stiffness = PreFe((2*e_s+e_b-10)*6+3) ./ parasitic_MMM(:,2);

stiffness = [y_stiffness,z_stiffness];

%create objective function
[max_force, max_idx] = max(RF_x_positions);
[min_force, min_idx] = min(RF_x_positions);

%desired forces
desired_max_force = 5;

%weight for components, position if needed
weight   = 1;
```

```
weight_1 = 1e6;
weight_2 = 1e5;

% Desired mean for RF_x_positions
desired_mean_RF = 0.15;

%calculation of the objective components
component1 = weight * min(abs(y_stiffness)); % check if y or z stiffness
component2 = weight_1 * (max_force - desired_max_force)^2;
component3 = weight_2 * (mean(RF_x_positions) - desired_mean_RF)^2;

 %combination of the objective components
 objective = -component1  + component2 + component3;

    catch ME
        disp(['Error in Param_opt: ' ME.message]);
        objective = NaN; % Return NaN when there's an error
    end

    fprintf('Current Objective Value: %.4f\n', objective);

end
```

D.2. Optimization Single-run

Main code for the single-run optimizer:

```
%% Fmincon

%define initial guess for the parameters

x0 = [0.0016 0.009 0.115 0.0175 0.00125 0.035];
%       TBB     V       LB

%define constraints
A = [];  % Linear inequality constraints
b = [];  % Linear inequality constraints
Aeq = [];  % Linear equality constraints
beq = [];  % Linear equality constraints
lb = [1.4e-3 7e-3 110e-3 15e-3 1e-3 30e-3];   %lower bounds
ub = [1.8e-3 10e-3 120e-3 20e-3 1.5e-3 40e-3];  % Upper bounds

tic;

% Call fmincon

options = optimoptions(@fmincon,'Display','iter-detailed');

[optimal_variables, fval ,exitflag] = fmincon(@Param_opt_3runs, x0, A, b, ...
    Aeq, beq, lb, ub,[], options);

%print the results
fprintf('The optimal parameters are: %.4f,%.4f,%.4f,%.4f,%.4f,%.4f\n',
    optimal_variables);
fprintf('The objective value is: %.4f\n', fval);

elapsedTime = toc;
fprintf('Time taken for optimization: %.2f seconds\n', elapsedTime);
```

D.3. Optimization Multistart

Main code for the Multistart object optimizer:

```
%% run optimization

lb = [1.4e-3 8e-3 110e-3 15e-3 1e-3 30e-3]; %lower bound

ub = [1.8e-3 10e-3 120e-3 20e-3 1.5e-3 40e-3]; %upper bound

x0 = [0.0016   0.009 0.115 0.0175    0.00125 0.035]; %initial guess


opts = optimoptions(@fmincon,'Algorithm','sqp');

problem = createOptimProblem('fmincon','objective',@Param_opt_3runs,'x0',x0, ...
    'lb',lb,'ub',ub,'options',opts);

ms = MultiStart();

[x,fval,exitflag,output,solutions] = run(ms,problem,4)

save("optimresults.mat")

fprintf('The optimal parameters are: %.4f,%.4f,%.4f,%.4f,%.4f,%.4f\n', x);
fprintf('The objective value is: %.4f\n', fval);
```

Bibliography

[1] Liang X. Shao S and X. Li. “Experimental investigation of particle dispersion in cleanrooms of electronic industry under different area ratios and speeds of fan filter units”. In: *Journal of building engineering* (2021). DOI: 10.1016/J.JOBE.2021.102590.

[2] T. Jiang and K. Jiang. “Numerical analysis of a hydrodynamic air bearing with electromagnetic assistance”. In: *Journal of Engineering Triboligy* 237 (6 2022). DOI: 10.1177/13506501221100617.

[3] S. Ro and J. Park. “A Compact Ultra-precision Air Bearing Stage with 3-DOF Planar Motions Using Electromagnetic Motors”. In: *Journal of precision engineering and manufacturing* 12 (2011), pp. 115–119. DOI: 10.1007/s12541-011-0014-y.

[4] Compliant Mechanism Research Group Brigham Young University. *Compliant mechanisms explained*. Available at https://www.compliantmechanisms.byu.edu/about-compliant-mechanisms.

[5] A. B. Mackay et al. “Metrics for Evaluation and Design of Large-Displacement Linear-Motion Compliant Mechanisms”. In: *Journal of Mechanical Design* 134.1 (2012), p. 011008. DOI: 10.1115/1.4004191.

[6] Shuvam Senapati. *FASCINATING WORLD OF COMPLIANT MECHANISMS*. Available at https://ieee.nitk.ac.in/blog/compliant-mechanisms. 2017.

[7] Solehuddin Shuib, M.I.Z. Ridzwan, and A.H. Kadarman. “Methodology of Compliant Mechanisms and its Current Developments in Applications: A Review”. In: *Compliant Mechanism Applications* (2007). ISSN: 1546-9239. DOI: 10.3844/ajassp.2007.160.167.

[8] Kee Bong Choi and Doo Hyeong Kim. “Monolithic parallel linear compliant mechanism for two axes ultraprecision linear motion”. In: *Review of Scientific Instruments* 77.6 (2006). ISSN: 00346748. DOI: 10.1063/1.2207368.

[9] Larry L. Howell. *Compliant Mechanisms*. John Wiley & Sons, 2001.

[10] CMDE Labs. *Compliant Mechanism: Advantages & Challenges*. Available at https://cmdelabs.medium.com/compliant-mechanism-advantages-challenges-27ff4a0e0566. 2021.

[11] Z. Zhou et al. “A bistable mechanism with linear negative stiffness and large in-plane lateral stiffness: design, modeling and case studies”. In: *Mech. Sci* (2020). DOI: 10.5194/ms-11-75-2020.

[12] L. Yan, S. Lu, and P. Liu. “Development of a Fully Compliant Bistable Mechanism Based on Circular Beams with Enhanced Pitch Stiffness”. In: *Appl. Sci* (2023). DOI: 10.3390/app13031642.

[13] Shannon A. Zirbel et al. “Bistable mechanisms for space applications”. In: *PLoS ONE* 11.12 (Dec. 2016). ISSN: 19326203. DOI: 10.1371/journal.pone.0168218.

[14] A. Alqasimi, C. Lusk, and J. Chimento. “Design of a Linear Bistable Compliant Crank–Slider Mechanism”. In: *J. Mechanisms Robotics.* (2016). DOI: 10.1115/1.4032509.

[15] D.M. Brouwer J.Rommers M. Naves and J.L. Herder. “A large range spatial linear guide with torsion reinforcement structures”. In: *Journal of Mechanics and Robotics* (2021). DOI: 10.1115/1.4052971.